Article

Cell

Genetic and Mechanical Regulation of Intestinal Smooth Muscle Development

Graphical Abstract

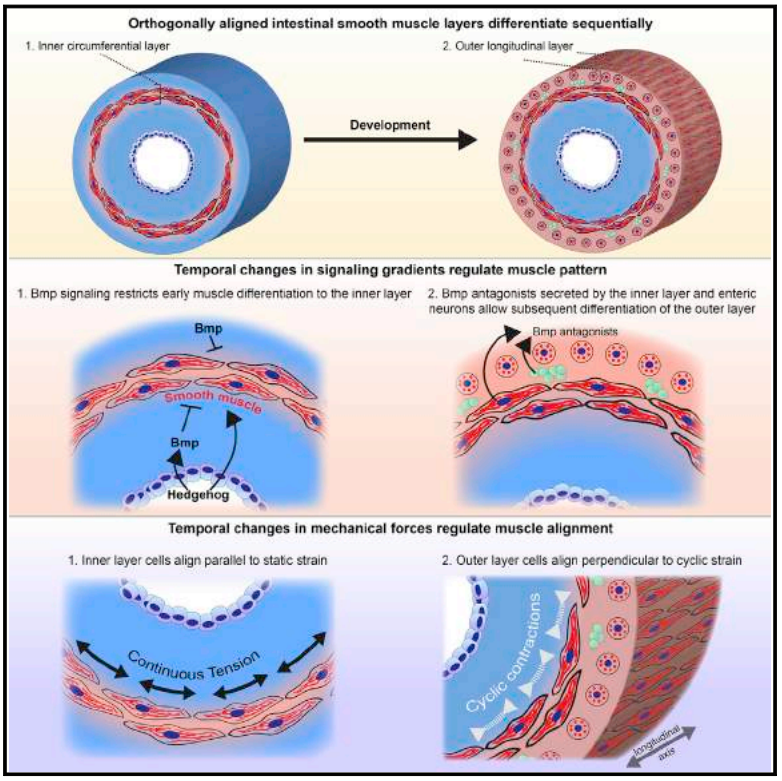

Highlights

- Gut smooth muscle is patterned by molecular signals and aligned by mechanical forces
- Hedgehog and Bmp signaling control spatiotemporal differentiation of muscle layers
- Differential growth generates static strain that aligns the inner circumferential layer
- Cyclic contractions of the circumferential layer orient the longitudinal layer

Authors

Tyler R. Huycke, Bess M. Miller, Hasreet K. Gill, Nandan L. Nerurkar, David Sprinzak, L. Mahadevan, Clifford J. Tabin

Correspondence

tabin@genetics.med.harvard.edu

In Brief

Gut smooth muscle patterning entails mechanical strain that orients the first layer circumferentially, and when formed, it spontaneously contracts to align the second layer longitudinally.

Huycke et al., 2019, Cell *179*, 90–105
September 19, 2019
https://doi.org/10.1016/j.cell.2019.08.041

CellPress

Cell

Article

Genetic and Mechanical Regulation of Intestinal Smooth Muscle Development

Tyler R. Huycke,[1] Bess M. Miller,[2] Hasreet K. Gill,[1] Nandan L. Nerurkar,[3] David Sprinzak,[4] L. Mahadevan,[5,6,7,8] and Clifford J. Tabin[1,9,*]

[1]Department of Genetics, Blavatnik Institute, Harvard Medical School, Boston, MA 02115, USA
[2]Department of Orthopedic Surgery, Brigham and Women's Hospital, Boston, MA 02115, USA
[3]Department of Biomedical Engineering, Columbia University, New York, NY 10027, USA
[4]Department of Biochemistry and Molecular Biology, George S. Wise Faculty of Life Science, Tel Aviv University, Tel Aviv, Israel
[5]School of Engineering and Applied Sciences, Harvard University, Cambridge, MA 02138, USA
[6]Department of Organismic and Evolutionary Biology, Harvard University, Cambridge, MA 02138, USA
[7]Department of Physics, Harvard University, Cambridge, MA 02138, USA
[8]Kavli Institute for Bionano Science and Technology, Harvard University, Cambridge, MA 02138, USA
[9]Lead Contact
*Correspondence: tabin@genetics.med.harvard.edu
https://doi.org/10.1016/j.cell.2019.08.041

SUMMARY

The gastrointestinal tract is enveloped by concentric and orthogonally aligned layers of smooth muscle; however, an understanding of the mechanisms by which these muscles become patterned and aligned in the embryo has been lacking. We find that Hedgehog acts through Bmp to delineate the position of the circumferentially oriented inner muscle layer, whereas localized Bmp inhibition is critical for allowing formation of the later-forming, longitudinally oriented outer layer. Because the layers form at different developmental stages, the muscle cells are exposed to unique mechanical stimuli that direct their alignments. Differential growth within the early gut tube generates residual strains that orient the first layer circumferentially, and when formed, the spontaneous contractions of this layer align the second layer longitudinally. Our data link morphogen-based patterning to mechanically controlled smooth muscle cell alignment and provide a mechanistic context for potentially understanding smooth muscle organization in a wide variety of tubular organs.

INTRODUCTION

The vertebrate gastrointestinal (GI) tract comprises an endodermal epithelium surrounded by discrete layers of smooth muscle derived from splanchnic mesoderm. In the embryo, these muscles physically constrain the growth of undifferentiated mesenchyme and endoderm to drive villus formation (Shyer et al., 2013) and intestinal stem cell localization (Shyer et al., 2015). From fetal through adult life, the coordinated peristaltic contractions of these muscles provide the essential function of propelling digested contents through the gut. The layers of smooth muscle differentiate sequentially during development. As visualized by α-smooth muscle actin (SMA) immunostaining, an inner layer of circumferentially aligned muscle is established prior to an outer longitudinally aligned layer (Gabella, 2002; Kedinger et al., 1990; McHugh, 1995; Figures 1A, S1A, and S1B). As they differentiate, the muscle fibers of each layer align in orthogonal orientations. Although there is a clear descriptive understanding of the sequence of events in gut smooth muscle formation, how the muscle layers are specified in the appropriate location, with the correct orientation, and at the right time remains unresolved.

Several signals have been implicated as broadly affecting muscle differentiation in the developing gut. In particular, Sonic (Shh) and Indian (Ihh) Hedgehog, which are expressed by the endoderm, signal in a paracrine manner to the surrounding mesenchyme to control its differentiation (Bitgood and McMahon, 1995; Kolterud et al., 2009; Roberts et al., 1995). Paradoxically, reports in the mouse and chick suggest that Hedgehog (Hh) signaling plays opposite roles in regulating smooth muscle myogenesis in the two species. Genetic studies in the mouse indicate that Hh signaling is required for and induces smooth muscle formation (Huang et al., 2013; Mao et al., 2010; Ramalho-Santos et al., 2000). This activating role of Hh seems to be through direct activation of *Myocardin*, a master regulator of smooth muscle differentiation (Cotton et al., 2017; Wang et al., 2003; Zacharias et al., 2011). Conversely, tissue grafting experiments and pharmacological modulation of the Hh pathway in chick explant culture suggest that the pathway inhibits smooth muscle differentiation (Sukegawa et al., 2000).

A second secreted factor that has been reported to affect smooth muscle formation in the gut is bone morphogenetic protein 4 (Bmp4). Overexpression of Bmp4 or hyperactivation of the Bmp pathway in the chick stomach (gizzard) or hindgut results in mesenchymal thinning and decreased smooth muscle, indicating that Bmp signaling inhibits myogenesis in this context (De Santa Barbara et al., 2005; Roberts et al., 1998; Smith et al., 2000). Intriguingly, in the early gut, *Bmp4* is activated by and dependent on high threshold concentrations of Hh adjacent to the endoderm (Roberts et al., 1995), suggesting a level of integration between the two pathways.

Beyond being placed in the correct location, the proper alignment of each layer of smooth muscle cells is critical for their physiological function. The collective orientation of each layer determines the axis along which contractile compressive forces are generated, producing epithelial buckling during gut development and peristaltic movement through the mature GI tract. Although the mechanisms orienting the orthogonal muscle layers in the gut are unknown, studies with cultured muscle cells have given insight into the cues that can influence their orientation. In particular, *in vitro* studies have demonstrated the ability of fibroblastic cell types, including smooth muscle, to align in response to various mechanical stimuli. In general, static (continuous) stretch aligns cells parallel to the major axis of strain, whereas cyclic stretch aligns cells perpendicular to the strain axis (Buck, 1980; Eastwood et al., 1998; Faust et al., 2011; Kanda and Matsuda, 1994; Kim et al., 1999). The degree of alignment depends on parameters such as strain frequency, amplitude, and physical properties of the substrate to which the cells are attached (reviewed in Tamiello et al., 2016). This apparent general property of fibroblastic cells begs the question of whether mechanical cues within the early gut act to align nascent smooth muscle cells and their associated fibers. In support of this idea, the early gut tube is a mechanically active environment because the circumferential layer itself compresses the inner tissues (Shyer et al., 2013) and also exhibits spontaneous contractions (Chevalier et al., 2017; Roberts et al., 2010), although a role of these contractile forces in morphogenesis has been unexplored.

Here we gain insight into these important open questions regarding gut patterning and morphogenesis. We start by addressing the mechanisms responsible for specifying the timing and location of smooth muscle layer formation and then investigate the concurrent mechanisms underlying the cellular orientation of each layer.

RESULTS

Levels of Hedgehog Signaling Regulate Differentiation of the Inner Smooth Muscle Layer

There is strong evidence that Hh signaling affects gut smooth muscle myogenesis; however, as noted above, there are contradictory data regarding the directionality of its influence (Mao et al., 2010; Sukegawa et al., 2000). To reconcile these conflicting reports, we posited that Hh signaling might act in a threshold-dependent manner during patterning of the circumferential muscle layer, inhibiting smooth muscle formation at high concentrations adjacent to the endoderm but activating it at lower concentrations farther away, which would generate the observed concentric ring of circumferential muscle a small distance removed from the endoderm. To test this, we cultured chick midgut explants from embryonic day 5 (E5), prior to formation of the inner muscle layer (Shyer et al., 2013), for 72 h while pharmacologically titrating levels of Hh signaling (Figures 1B–1E and S1C–S1F). Control explants developed inner circumferential muscle comparable with *in vivo* conditions, with smooth muscle cells forming a ring surrounding the endoderm and undifferentiated subepithelial mesenchyme (Figures 1A and 1B). Addition of 10 μM cyclopamine, a Hh signaling inhibitor, completely blocked Hh signaling (as visualized by loss of expression of its downstream target *PTCH1*) along with smooth muscle differentiation, supporting the notion that Hh is required for smooth muscle differentiation and consistent with the published mouse genetic studies. With 1 μM cyclopamine, Hh signaling levels were dampened but not eliminated, and muscle differentiation persisted adjacent to the endogenous source of Hh production in the endoderm, the mesodermal domain with the highest levels of Hh signaling. Conversely, increasing levels of Hh signaling via addition of 250 nM recombinant Shh expanded the domain of smooth muscle. However, increasing the level of Hh activity even further by treatment with 500 nM Shh or implantation of a Shh-soaked bead, resulted in a lack of smooth muscle, consistent with previous chick studies (Figures 1B–1E and S1C–S1G).

Hedgehog Acts through Bmp Signaling to Inhibit Smooth Muscle

In principle, Hh activity could achieve these opposing effects on smooth muscle differentiation as a classic morphogen, driving distinct cellular responses in a concentration-dependent manner. However, an alternative model, where some of the observed effects of Hh might be indirect and mediated by a secondary signal, was suggested by the fact that a second secreted signal, Bmp4, is a known target of Hh in the developing GI tract (Roberts et al., 1995) and has been shown previously to limit smooth muscle differentiation and growth in stomach and hindgut mesenchyme (De Santa Barbara et al., 2005; Roberts et al., 1998). In particular, we posited that the observed inhibitory effect caused by high Hh signaling levels might be mediated through Bmp4. Indeed, in the developing midgut, *BMP4* is expressed in cells adjacent to the endoderm that receive the highest amounts of Hh; its expression increases throughout the mesenchyme in response to Hh in a dose-dependent manner (Figures 2A, 2B, and S2A), and these Hh-dependent alterations to *BMP4* expression positively correlate with levels of Bmp signaling activity, as assessed by phospho-Smad1/5/9 immunostaining (Figures 2C, 2D, S2B, and S2C). Moreover, treatment of midgut explants with recombinant Bmp4 reduces smooth muscle formation, whereas sustained overexpression of Noggin, a Bmp antagonist, induces ectopic subepithelial smooth muscle (Figures 2C–2E, S2B, and S2C). We directly tested whether the inhibitory effect of Hh on muscle differentiation is mediated through Bmp signaling by co-incubating explants with 500 nM Shh (which, on its own, blocks smooth muscle formation) along with Noggin, resulting in a loss of detectable Bmp activity and rescuing smooth muscle differentiation (Figures 2C, 2D, S2B, and S2C).

To further probe the regulation of smooth muscle differentiation by Hh and Bmp, we examined the expression of Myocardin (*MYOCD*) and Myocardin-related transcription factors (*MRTFA/B*), master transcriptional regulators of smooth muscle myogenesis (Wang et al., 2003). Treatment of E5 explants for 72 h with 500 nM Shh significantly downregulated the expression of *MYOCD* and *MRTFA/B* as well as their targets *ACTA2* (αSMA) and *TAGLN* (Sm22α), whereas co-treatment of explants with Noggin restored the expression levels of *MRTFA/B*, *ACTA2*, and *TAGLN*, matching the changes to smooth muscle patterning we observed at the protein level (Figures 2F and S2D). A time course

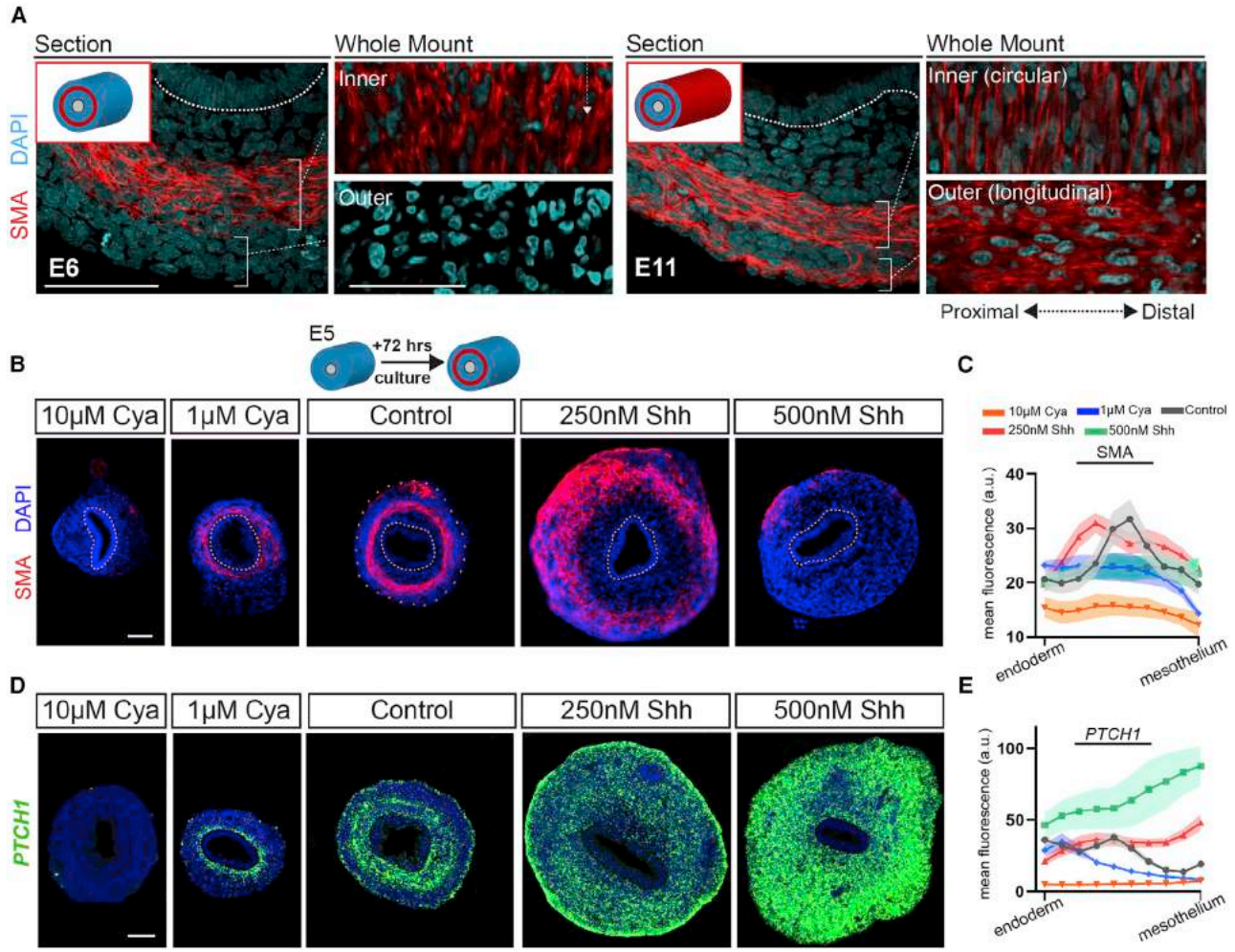

Figure 1. Hedgehog Signaling Patterns Circumferential Smooth Muscle in a Concentration-Dependent Manner

(A) Transverse cross-sections and corresponding whole-mount images of smooth muscle differentiation and alignment in the chick midgut. At E6, the nascent inner layer first appears and aligns in the circumferential direction, perpendicular to the gut proximal-distal axis. At E11, the outer layer differentiates and aligns longitudinally, parallel to the proximal-distal axis.

(B) Cross-sections of explanted midguts treated with cyclopamine or recombinant Shh.

(C) Quantification of the smooth muscle actin (αSMA) pattern across the radial thickness of the gut tube based on immunofluorescence from cross-sections in (B). The endoderm boundary is highlighted by a white dashed line, and the mesothelium boundary is highlighted by an orange dashed line in the (B) control sample.

(D) Fluorescence *in situ* hybridization (FISH) of *PTCH1* expression in sections equivalent to (B).

(E) Quantification of the *PTCH1* FISH signal across the radial thickness as in (C).

Images are representative of at least 4 replicate guts per treatment. Error bars are mean ± SEM. Scale bars, 50 μm.

See also Figure S1.

analysis in the presence of 500 nM Shh revealed that, in contrast to its observed later inhibitory role, the high dose of Shh initially activates expression of *MYOCD* (but not *MRTFA/B*), *ACTA2*, and *TAGLN* after 12 h, supporting previous reports that Myocardin is a direct target of Hh signaling within intestinal mesenchyme (Figure S2E; Cotton et al., 2017; Zacharias et al., 2011). Additionally, these results also indicate that the inhibitory effect of high Shh on muscle formation is mediated through a secondary factor. In accordance with this notion, *BMP4* expression is also induced by high concentrations of Shh after 12 h, and addition of recombinant Bmp4 alone leads to downregulation of *MYOCD*, *MRTFA/B*, *ACTA2*, and *TAGLN* (Figures 2G, S2D, and S2E). Combined with the fact that Hh inhibition via cyclopamine treatment reduces *MYOCD* but not *MRTFA/B* expression levels (Figure 2F), these data suggest that *MYOCD* and, thus, smooth muscle differentiation is initially induced by Hh but secondarily repressed by Bmp4 (itself induced by high levels of Hh). Taken together, these results resolve previous discrepancies and further support a model in which Hh signaling is required for smooth muscle differentiation and additionally acts through Bmp signaling in a concentration-dependent manner to locally repress factors known to regulate smooth muscle differentiation in subepithelial mesenchyme, thereby patterning the first-forming inner layer of smooth muscle (Figure 2H).

The foregoing model provides an explanation for the spatial separation of the inner circumferential smooth muscle ring from the endodermal layer; however, it leaves unexplained why this layer does not extend radially to the outer boundary of the gut mesoderm. Our observation that Bmp antagonism induces precocial smooth muscle within the outer mesenchyme suggests that Bmp signaling also acts to inhibit smooth muscle differentiation lateral to the first forming ring of muscle (Figures 3A, 3B, S2F, S2G, and S3A). This can be explained by the fact that *BMP2* and *BMP7* are expressed by mesothelial cells adjacent to the outer mesenchyme (Figure 3C). There are, therefore, two sources of Bmp activity, at the inner and outer edges of the developing gut mesenchyme, which would be expected to establish opposing oriented gradients with a low-Bmp-activity sweet spot in the middle, where Hh activity is free to induce the first smooth muscle layer. Indeed, just prior to muscle differentiation at E4, a gradient of pSmad1/5/9 is seen within the mesenchyme and is highest in in the domain where *BMP4* is expressed adjacent to the endoderm and lower where muscle will form (Figures S4A–S4D).

Localized Downregulation of Bmp Activity Specifies the Timing and Location of Outer Smooth Muscle Differentiation

When the first smooth muscle layer has formed, the domains of Bmp inhibition need to be shifted if additional mesenchymal tissue is to differentiate into subsequently forming smooth muscle layers. In support of this, Bmp signaling activity negatively correlates with outer longitudinal muscle formation; it is high in the outer mesenchyme during and after formation of the first layer and becomes focally downregulated within this region prior to and during outer longitudinal muscle formation at E10–E12 (Figure S4). This downregulation of Bmp signaling appears to be important because overexpression of Bmp2 in this domain reduces muscle differentiation at E13.5, a time when it is well formed in controls (Shyer et al., 2013; Figures 3D, 3E, and S3B). At later stages, Bmp activity increases within the inner layer after it has formed (Figure S4), consistent with a second, later role in smooth muscle cell maturation (Notarnicola et al., 2012).

One potential mechanism by which Bmp activity could be focally reduced in the outer mesenchyme to allow its differentiation into muscle would be through localized expression of Bmp antagonists. Indeed, we observe that *NOGGIN* is expressed by both the neural crest-derived enteric neurons adjacent to the outer layer and by the newly differentiated inner circumferential muscle at E8–E9, just prior to the emergence of outer longitudinal muscle (Figures 3C and S3C). Given the proximity of the enteric neurons to the outer mesenchyme, we first tested whether the presence of neural crest-derived cells was required for outer layer formation. However, neither ablation of neural crest cells nor culturing of aneural explants affected outer layer differentiation or alignment (Figures S3D and S3E), consistent with previous studies (Lecoin et al., 1996; Nagy et al., 2016).

Because *NOGGIN* is also expressed by inner circumferential muscle, we hypothesized that tissue-level redundancy may compensate for loss of the ablated neural crest. To more conclusively test whether Bmp antagonism is required for outer layer differentiation, we performed tissue-specific loss-of-function experiments in the mouse, which shows spatiotemporal patterning of smooth muscle similar to the chick (Shyer et al., 2015; Walton et al., 2016; Figures S1A and S1B). Using both mesoderm (*Twist2-cre*) and neural crest (*Wnt1-cre*) drivers, we conditionally deleted the Bmp antagonists *Noggin* and *Gremlin1*, which are expressed by neurons and inner circumferential muscle at E13.5, just prior to outer layer differentiation at E14.5 (Figures 3C and S3G). Although mice lacking *Noggin* and *Gremlin1* in either population individually had no intestinal phenotype, mice lacking both genes in mesoderm and neural crest together (*Twist2-cre, Wnt1-cre; Nog*$^{fl/fl}$*, Grem1*$^{fl/fl}$) showed hypoplastic differentiation of the longitudinal smooth muscle layer at E16, a time when this layer is well formed in controls (Walton et al., 2016; Figures 3F, 3G, S1A, S3F, and S3G). The lack of outer layer differentiation in mutants was mirrored by increased Bmp signaling activity within the outer mesenchyme (Figures 3F, 3G, and S3G). Notably, this phenotype appeared to be exclusive to the duodenum, indicating that there may be compensation in other regions by other Bmp antagonists expressed within the developing gut. Indeed, we observed localized expression of multiple Bmp antagonists within enteric neurons and mesoderm of the jejunum at the time of outer layer smooth muscle differentiation (Figure S3H), suggesting functional redundancy. Together, these data from both chick and mouse support a model wherein Bmp activity in the early gut tube maintains the outer and inner mesenchyme in an undifferentiated state. Then, spatiotemporally controlled inhibition of Bmp signaling mediated by antagonists derived from the inner circumferential muscle and enteric neurons allows timely outer longitudinal muscle formation (Figure 3H).

Strain Generated by Differential Growth Aligns Circumferential Smooth Muscle

For proper functioning of the gut, it is critical that the smooth muscle layers not only form in the right spatial location but also with the proper cellular orientation. Prior *in vitro* and theoretical work has demonstrated that fibroblasts and smooth muscle cells from other organs (e.g., vascular smooth muscle) respond to static mechanical stretch by aligning with the major axis of strain (Eastwood et al., 1998; Kanda et al., 1992; Rens and Merks, 2017). This appears to be a general property of smooth muscle cells in culture because we found that cultured embryonic intestinal smooth muscles also align parallel to static stretch (Figure S5A). The acquisition of cellular alignment within each layer occurs concomitantly with smooth muscle differentiation, leading us to hypothesize that mechanical stimuli acting on the cells as each layer differentiates might control their unique orientations (Figures S5B and S5C). To see whether static strain was present within the developing gut, we employed a simple test where a radial cut was made along a segment of the gut tube. If residual strains were present, then the tube would be expected to open up, whereas a tube devoid of such strains would remain in its original cylindrical shape (albeit with a cut along one side). The degree of the angle to which the tube opens reflects the degree of stress within the tube prior to cutting (Fung, 1991). When cut radially at E5, the midgut indeed opens circumferentially, revealing the

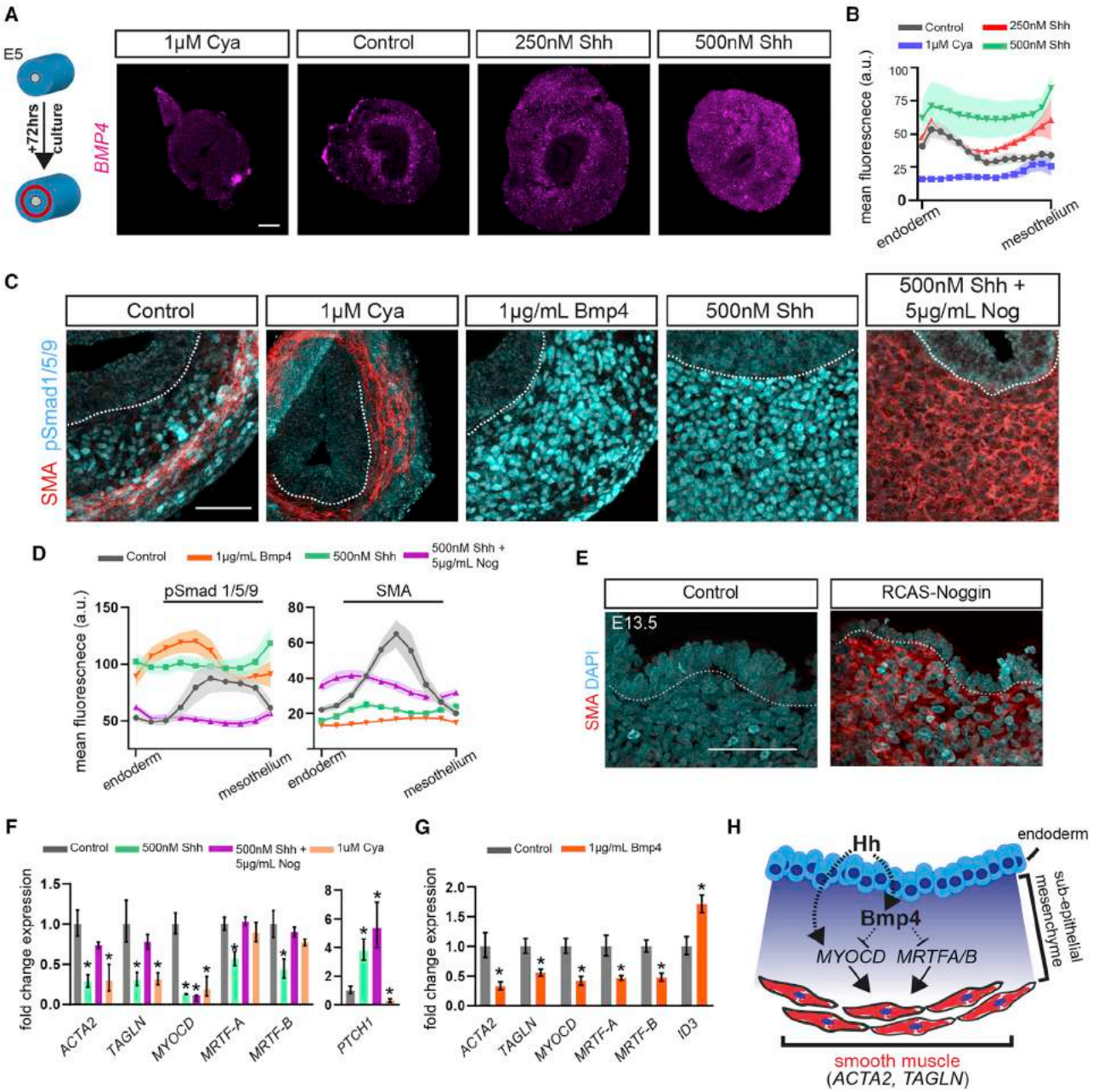

Figure 2. Hedgehog Acts through Bmp Signaling to Inhibit Subepithelial Smooth Muscle

(A) FISH of *BMP4* expression in midgut explants treated with cyclopamine or recombinant Shh from E5 for 72 h.

(B) Quantification of radial expression of *BMP4* from images in (A).

(C) Sections from explanted midguts cultured as in (A) and immunostained for pSmad1/5/9. Dotted lines denote the endoderm-mesenchyme boundary.

(D) Quantification of the radial pattern of SMA and nuclear pSmad1/5/9 immunofluorescence from sections in (C).

(E) Sections from the jejunum of E13.5 chick midguts electroporated with RCAS-Noggin at E2.5.

(F) Gene expression levels determined by qPCR from E5 guts cultured for 72 h with the noted treatments. Fold change expression is relative to *GAPDH.* Error bars are mean + SEM. *p < 0.05 by t test.

(G) qPCR data from E5 guts treated for 12 h with 1 μg/mL Bmp4.

(H) Model for Hh-Bmp-mediated patterning of the circumferential layer. Hh (both Sonic and Indian ligands) is expressed by the endoderm and activates Bmp4 expression in the subjacent non-muscle mesenchyme, where its concentration is highest. Bmp4 subsequently acts at high concentrations to inhibit smooth muscle formation in this subepithelial compartment through repression of *MYOCD* and *MRTFA/B*, whereas Hh acts through promoting *MYOCD* expression to induce muscle formation at a distance farther away, where inhibitory Bmp levels are lower.

Images are representative of at least 4 replicate guts per treatment. Error bars are mean ± SEM. Scale bars, 50 μm.

See also Figure S2.

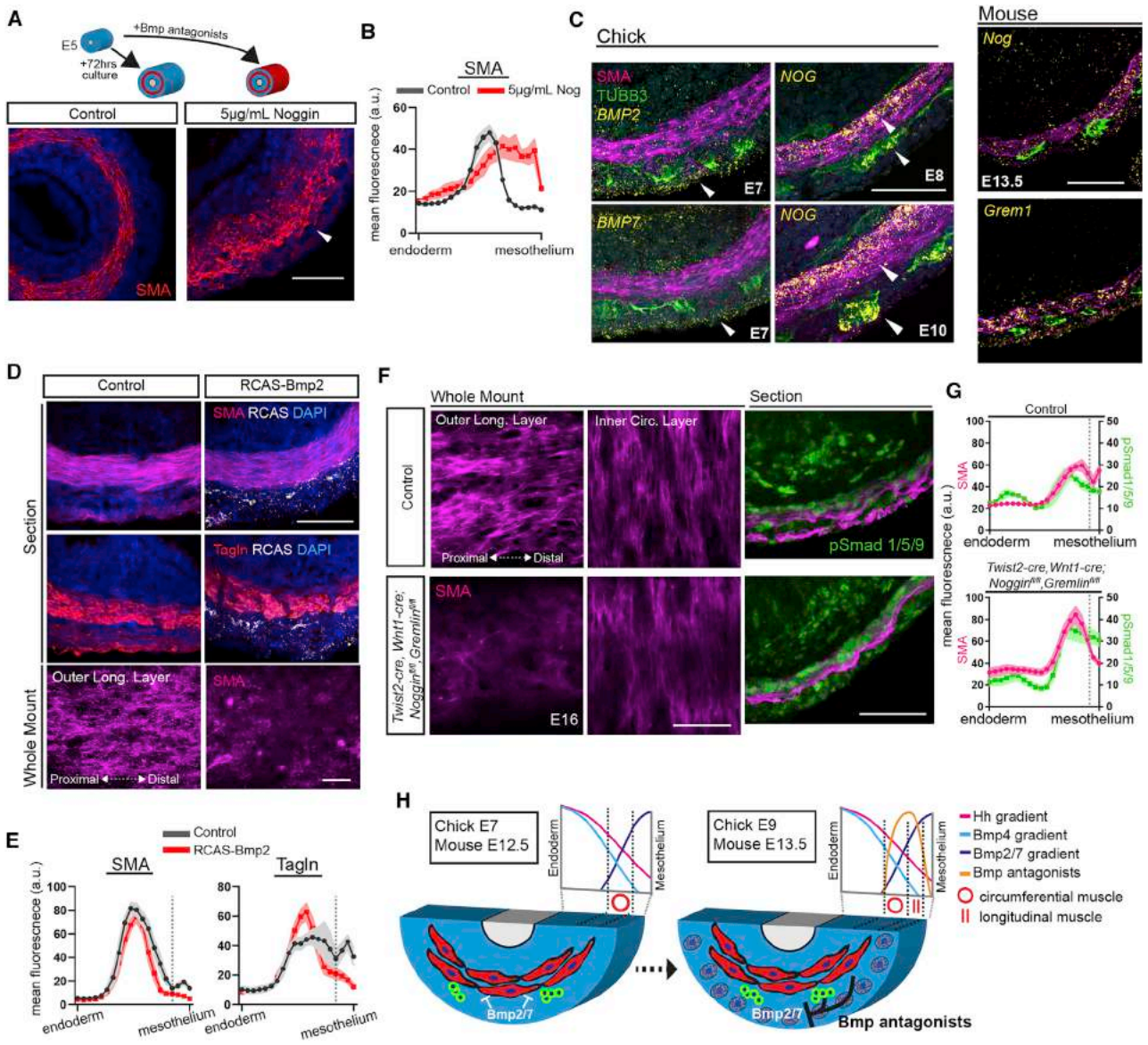

Figure 3. Outer Longitudinal Smooth Muscle Differentiation Depends on Local Bmp Inhibition

(A) Cross-section of control and Noggin-treated midgut explants; the arrowhead denotes precocial muscle (representative of 6 replicate guts).

(B) Quantification of the radial smooth muscle pattern based on SMA staining from (A).

(C) FISH of *BMP2/7* in the midgut, showing expression in mesothelium (left arrowheads) and *NOG* expression in neurons and muscle (right arrowheads). Right: FISH of *Nog* and *Grem1* on mouse duodenal sections.

(D) Section and whole-mount immunofluorescence of RCAS-Bmp2 and control mock-electroporated jejunal midguts segments stained with SMA or TagIn (representative of 5 or more guts per treatment). Note that the electroporations performed in early lateral plate mesenchyme tend to more effectively target the outer mesenchyme.

(E) Quantification of the radial smooth muscle pattern from the experiment in (D). The dashed gray line denotes the boundary occupied by enteric neurons between the inner (to the left) and outer (to the right) muscle layers.

(F) Immunostained E16 mouse duodenum in whole mount and section (representative of 6 double mutants).

(G) Quantification of the radial smooth muscle pattern and nuclear pSmad1/5/9 from sections in (F). The dashed gray line denotes the boundary between muscle layers.

(H) Model of outer layer muscle development. After formation of the inner layer, there are two opposing Bmp gradients that inhibit muscle formation within the inner and outer mesenchyme. Just prior to and during the formation of the outer longitudinal layer, Bmp antagonists are expressed by myenteric neurons and the inner muscle layer, reducing Bmp activity locally within the outer layer of mesenchyme and allowing muscle differentiation.

Error bars are mean ± SEM. Scale bars, 50 μm.

See also Figures S1, S2, S3, and S4.

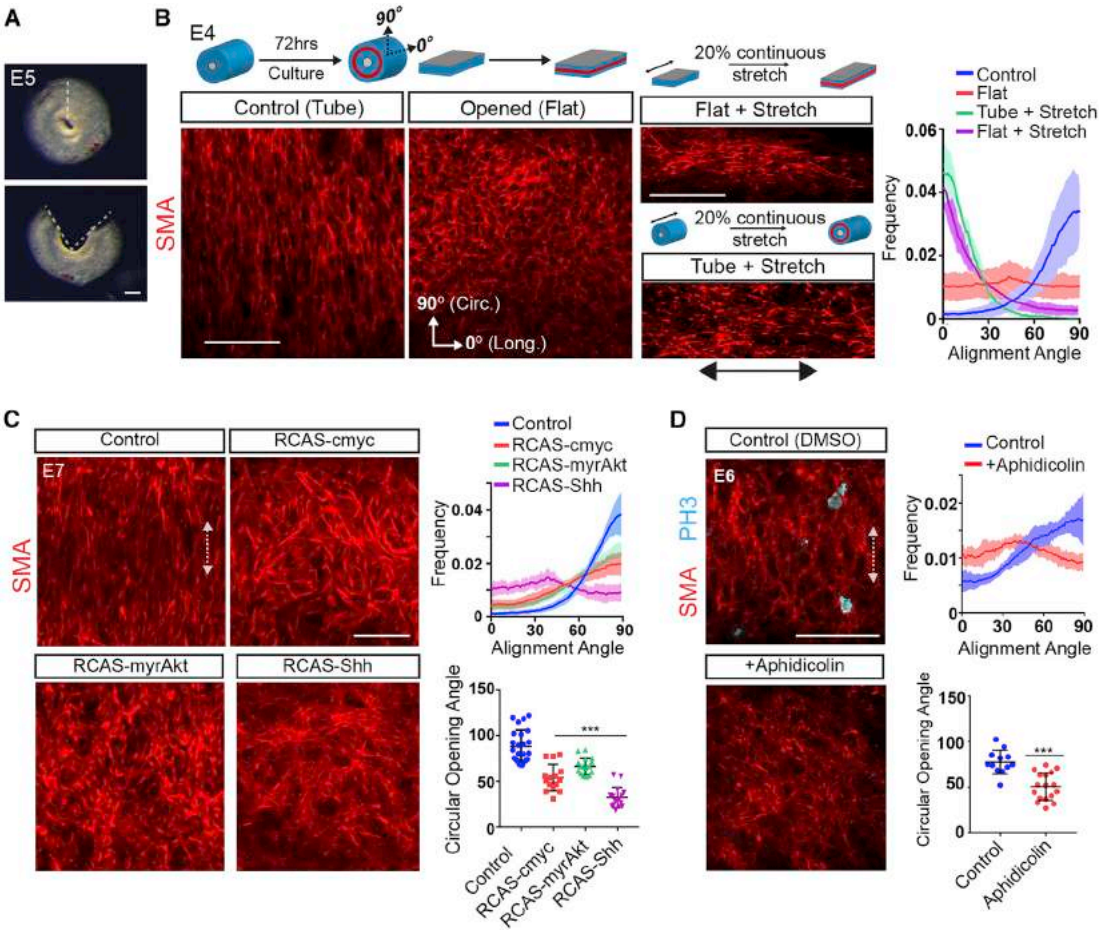

Figure 4. Continuous Strain from Differential Growth Aligns Inner Circumferential Smooth Muscle

(A) Jejunal section before and after a radial cut at E5 (prior to smooth muscle differentiation) to reveal the circumferential opening angle and residual strain.

(B) Immunostained whole-mount midgut explants following tubular or flat (zero-strain) culture and both conditions after application of longitudinal stretch. Quantification of actin alignment based on SMA staining. 90°, circumferential orientation; 0°, longitudinal.

(C) Whole-mount images of inner layer ileum segments following electroporation of viral constructs perturbing proliferation rates, along with alignment and opening angle measurements.

(D) Whole-mount images of midgut segments from embryos treated with aphidicolin or DMSO *in ovo*. Cell alignment quantifications are relative to the proximal-distal (long) axis of the gut.

Error bars are mean ± SD, ***$p < 0.001$ by two tailed t test. $n \geq 5$ measurements (alignment) and $n \geq 3$ (opening angle) per sample from at least 3 samples for each condition. Scale bars, 50 μm.

See also Figure S5.

presence of circumferential tension in the undifferentiated mesenchyme (Figure 4A). We then tested whether this residual strain is required for muscle alignment by culturing flat (zero-stress) midgut segments for 72 h starting at E4, prior to their differentiation and alignment. Compared with control midguts, in which smooth muscle aligned circumferentially, segments grown flat lacked muscle cell alignment (Figure 4B). Additionally, flat segments showed decreased expression of CNN1 and MYH11, markers of mature/contractile smooth muscle, suggesting that strain additionally plays a role in smooth muscle maturation (Figures S5D–S5F; Albinsson et al., 2004; Bono et al. 2016). Finally, when an exogenous 20% longitudinal stretch was applied to tubular or flat explants, cells aligned parallel to the stretch (perpendicular to their normal orientation), indicating that continuous strain is sufficient to align the inner layer (Figure 4B).

Residual strains arise in the gut because of differential growth along the radial axis as proliferation of the inner layers outpaces that of outer layers, resulting in a situation where the outer layers are circumferentially tensed and inner layers are compressed (Shyer et al., 2013; Figure S5G). Indeed, we found that cell cycle length is significantly shorter within the inner mesenchyme compared with the outer mesenchyme (Figures S5H–S5K). To see whether this differential growth is a major factor in aligning the circumferential muscle layer, we tested whether altering mesenchymal growth would perturb residual strain and, consequently, cell alignment by misexpressing factors known to change tissue growth rates. Viral overexpression of Shh,

myristoylated Akt (myrAkt), or cmyc each reduced cell cycle length in the outer mesenchyme, resulting in reduced differential growth, smaller opening angles, and decreased smooth muscle alignment at E7 (Figures 4C and S5I–S5M). Globally blocking proliferation with aphidicolin *in ovo* also resulted in reduced residual strain, again leading to a lack of smooth muscle alignment (Figures 4D and S5L). Together, these data support a model in which the orientation of strains within the undifferentiated mesenchyme aligns cells of the early-forming smooth muscle layer.

Cyclic Contractions of the Circumferential Layer Align the Outer Layer Longitudinally

We next tested whether residual strains were important for alignment of the subsequently differentiating longitudinal layer by culturing flat, cut-open guts at the time when the second smooth muscle layer forms. However, we found no perturbation in the alignment of either the already differentiated circular or forming longitudinal smooth muscle (Figure S6A). These results suggest that, when established, the orientation of the smooth muscle cells is maintained irrespective of strain and, additionally, that the outer layer aligns via a different mechanism than the inner.

When considering potential mechanisms that could explain the orthogonal orientation of the second-forming smooth muscle layer, we drew from previous tissue engineering and theoretical analyses showing that, in the context of cyclic strain, cells tend to align perpendicular to the axis of major strain (Faust et al., 2011; Kim et al., 1999; Livne et al., 2014), a property we verified with cultured embryonic intestinal smooth muscle cells (Figure S5A). This behavior was intriguing in light of the observation that circular smooth muscle displays spontaneous cyclic contractions soon after it differentiates (Chevalier et al., 2017; Roberts et al., 2010). Indeed, analysis of calcium levels with a GCaMP6S reporter (Li et al., 2018) showed the presence of pulsatile calcium transients within the undifferentiated mesenchyme as early as E4. As the circumferential layer differentiates, these pulses transform into waves propagating in both directions along the length of the intestine that coincide with circumferential muscle contractions (Figures S6B–S6D; Videos S1 and S2). Given these observations, we hypothesized that cyclic contractions of the first layer may align cells of the outer layer orthogonally in the longitudinal direction (Coulombre and Coulombre, 1958). To test this, we cultured whole intestinal explants from E9, prior to outer smooth muscle differentiation and alignment, for 72 h while decreasing or increasing circumferential muscle contraction frequency. We took advantage of the fact that fetal smooth muscle contraction depends on the activity of L-type calcium channels and myosin light chain kinase (MLCK), with calcium transients propagated between the cells via gap junctions to generate the contractile waves (Chevalier, 2018; Schultz et al., 2003). Consistent with our hypothesis, preventing these contractions during formation of the outer layer with nifedipine (a calcium channel inhibitor), ML-7 (an MLCK inhibitor), or carbenoxolone (a gap junction inhibitor) inhibited alignment of the outer muscle layer, whereas increasing the contractile frequency using the L-type calcium channel activator (*S*)-(-)-BayK8644 enhanced alignment (Figures 5A, S6B, and S6E; Video S3). In addition, the myenteric neural plexus, which is situated between the inner and outer muscle layers and itself is not required for muscle alignment (Figures S3D and S3E), also showed perturbed organization in guts treated with nifedipine (Figure S6F), suggesting additional roles for muscle contraction in gut morphogenesis. Importantly, neither differentiation of the outer layer nor alignment of the already formed circular layer was significantly altered by these treatments.

To test whether cyclic strain is sufficient to align smooth muscle cells of the outer layer, we attempted to restore an aligned orientation to cells of this layer after blocking endogenous cyclic contractions with nifedipine by applying an exogenous cyclic stretch to whole midgut segments at frequency (0.1667 Hz) and strain (15%) values similar to those normally observed for *in vivo* spontaneous contractions (Figure S6G). Because the mechanical device we utilized applied a cyclic longitudinal stretch rather than the cyclic circumferential strain found *in ovo*, we expected that outer layer muscle cells would align circumferentially, perpendicular to the applied cyclic strain axis but orthogonal to their normal orientation. Indeed, this is what we saw near the ends of the explanted gut segment. Surprisingly, the longitudinal cyclic strain resulted in cells adopting a longitudinal orientation near the middle of the segment (Figure S6G). We reasoned that the observed longitudinal alignment in the center of cyclically stretched segments might be due to compressive strains transverse to the stretch axis (Weidenhamer and Tranquillo, 2013) because we observed narrowing of the gut diameter in this region. We therefore repeated the aforementioned cyclic stretch experiment while minimizing transverse compressive strain by intubating the lumen of midgut explants with a thin tungsten rod (Figure S6H). In contrast to our previous results, the outer smooth muscle layer of these explants displayed a high degree of circular orientation across the entire length of the cultured segment, rescuing alignment in the absence of endogenous contractions and displaying a strikingly perpendicular alignment to controls (Figure 5B). These data demonstrate that cyclic stretch is sufficient to align cells in the absence of contractions and support a model wherein spontaneous contraction of the early-forming circumferential layer is the mechanical cue that aligns the later-forming outer longitudinal layer.

Static and Cyclic Strains Align Helical Smooth Muscle in the Mouse Esophagus

Many tubular organs are enveloped by layers of orthogonally aligned smooth muscle, pointing to the potential of a general mechanism that might underlie smooth muscle alignment in multiple contexts; the first layer of smooth muscle to form always orients its fibers with respect to continuous strains in the developing tissue, whereas the second layer orients orthogonally to it, directed by spontaneous cyclic contractions of the first layer. An interesting test for this idea was presented by the mouse esophagus, which contains two smooth muscle layers but with orthogonal helical alignments rather than circumferential and longitudinal (Figure 6A). In support of our model, we identified the presence of two longitudinal strains present in the esophagus but absent from the small intestine that could potentially generate the helical alignment. First, when cut proximally at E12, prior to the alignment of the first muscle layer, the esophagus decreases in length, indicating the presence of

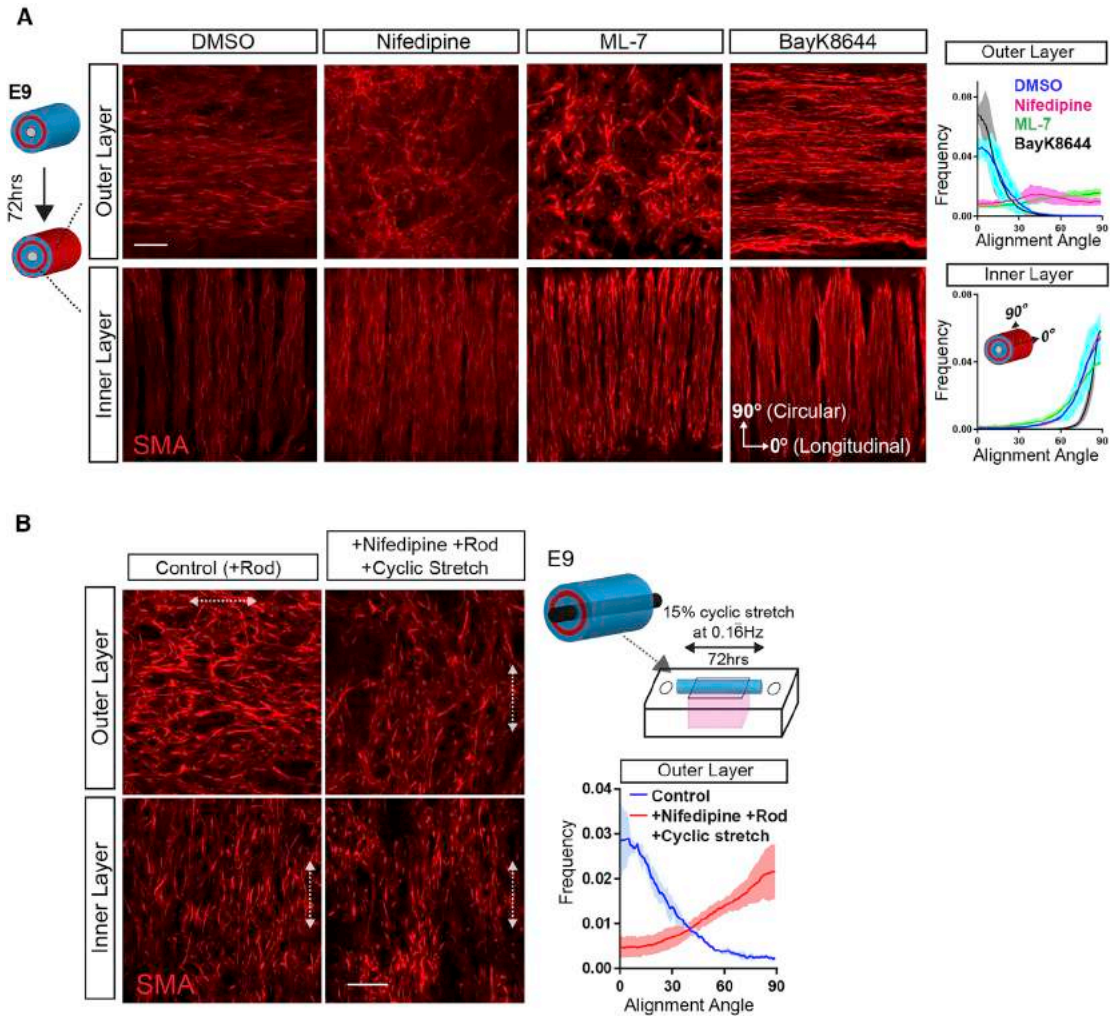

Figure 5. Cyclic Strain Aligns Outer Longitudinal Smooth Muscle

(A) Whole-mount images of immunostained inner and outer muscle layers and quantification of muscle alignment when contractions are blocked with nifedipine (100 μM) and ML-7 (45 μM) or increased with BayK8644 (1 μM) during outer layer differentiation.

(B) Whole-mount images and quantification of muscle alignment from midguts intubated with tungsten rods cultured with nifedipine and cyclically stretched longitudinally, compared with intubated unstretched controls. Arrows indicate axis of muscle alignment.

Quantifications of alignment, determined as in Figure 4, were obtained from 3 or more measurements per sample from at least 5 samples per condition. Inner and outer layers were distinguished by the presence of the neural plexus separating them. Error bars are mean ± SD. Scale bars, 50 μm.

See also Figures S5 and S6.

longitudinal stretch (Figures 6B and S7A). Second, when cut radially, the esophagus opens both circumferentially and longitudinally, indicating the presence of both circumferential and longitudinal residual strains (Figures 6C and S7B). Moreover, the esophagi of *Twist2-cre; Nog*$^{fl/fl}$*,Grem1*$^{fl/+}$ and *Twist2-cre; Nog*$^{fl/fl}$*, Grem1*$^{fl/fl}$ embryos, which develop a misaligned inner longitudinal muscle layer and an outer circumferential layer, show significantly increased longitudinal extensional strain and longitudinal residual strains (Figures 6A–6C, S7A, and S7B). As in the chick midgut, the alignment of the later-forming, orthogonally aligned outer layer of esophageal smooth muscle is dependent on the spontaneous contractions of the first (Figure 6D). Finally, using the chick midgut, we phenocopied the inverted, inside-out alignment of the *Nog/Grem* mutant esophageal muscle layers by first applying continuous longitudinal stretch during formation of the inner layer, causing it to align longitudinally. We then allowed the second layer to form in the absence of applied strain but with the misaligned muscle now contracting in the longitudinal direction. This induced formation of an outer circumferential layer reminiscent of the mutant esophagus and matches the predictions of our model (Figures 6E, 7A–7C, and S7C).

Spontaneous Contractions Are Required for Longitudinal Muscle Layer Alignment in the Ureter

We further tested this model in the context of a tubular organ outside of the GI tract, examining smooth muscle alignment in the mouse ureter. The first-forming circular layer of ureteral smooth muscle begins spontaneous contractions by E15.5, prior

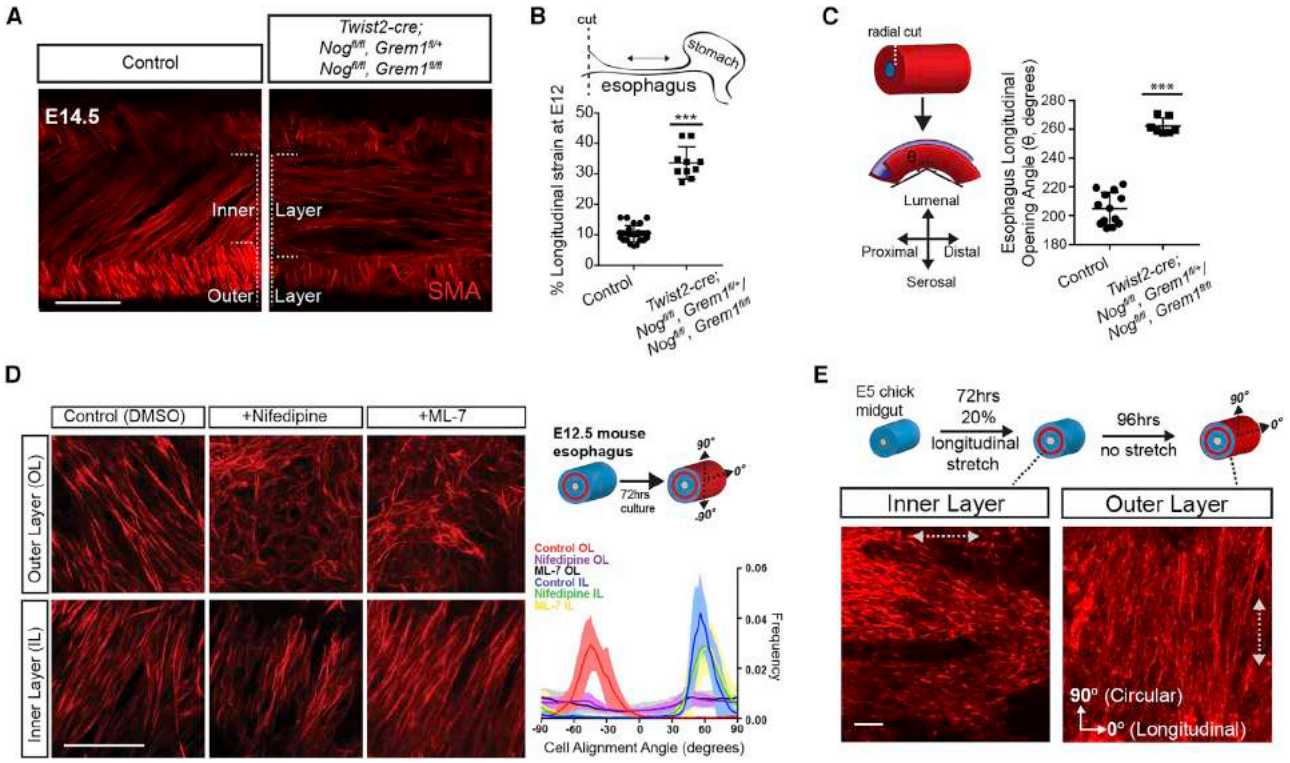

Figure 6. Mechanical Control of Helical Muscle in the Murine Esophagus

(A) Whole-mount projection of mouse esophagi from control and mutant embryos.

(B) Quantification of longitudinal tension in the esophagi of control and mutant embryos at E12.

(C) Quantification of the longitudinal opening angle of esophagi at E12, as defined by the reflex angle relative to the straight (uncut) tube ($\theta = 180^{\circ}$). Each point represents a different mouse.

(D) Whole-mount stain of muscle layers in mouse esophagi after culturing from E12.5 for 72 h with contraction inhibitors (nifedipine, 60 μM; ML-7, 45 μM). Quantifications of cell alignment were performed on at least 3 different regions for each of at least 6 separate explants per treatment.

(E) Whole mount of misaligned and inverted muscle layers of explanted chick midgut following application of exogenous stretch. Representative of 6 replicate guts. Error bars are mean ± SD, ***$p < 0.001$ by two tailed t test. Scale bars, 50 μm.

See also Figure S7.

to differentiation of an outer longitudinal layer that forms by E17.5 (Figure S7D). Again matching our results from the gut, blocking spontaneous ureteral contractions with nifedipine inhibits outer layer alignment (Figure S7E).

DISCUSSION

Understanding vertebrate myogenesis was one of the first problems in developmental biology investigated on the molecular level, with the discovery of MyoD by Lassar et al., (1986). Muscle development has remained an area of extremely active research ever since, and an enormous amount has been learned, from the role of myogenic genes in muscle cell specification to the control of satellite stem cells in repairing damaged muscle. Nonetheless, many fundamental problems regarding muscle patterning are still unanswered. Thus, questions such as, "why do your biceps have two heads and your triceps have three?"; "why do they form in the exact locations where they are found?"; and "why are muscle fibers oriented along the long axis of the limb instead of some other direction?" have remained largely unresolved. Here we address these questions for the set of smooth muscles in the midgut. We find that the location and timing of formation of the concentric layers of intestinal smooth muscle is achieved through a signaling cascade involving Hh, Bmp, and Bmp antagonists, whereas the proper orientation of these layers is established in response to unique mechanical forces present at different stages of intestinal development. Notably, both the differentiation and the orientation of later-forming layers depend on the formation of the first smooth muscle layer, a feature that may explain the relative orientation of smooth muscle layers in a variety of settings in the developing vertebrate embryo.

A Cascade of Signals Directing the Patterning of Sequential Smooth Muscle Layers

Previous studies have implicated Hh signaling as both a positive and negative regulator of GI smooth muscle (Mao et al., 2010; Sukegawa et al., 2000). Our results resolve these apparently contradictory results by demonstrating that these represent differential responses to different levels of Hh activity. However, rather than acting as a morphogen to induce different fates at specific concentrations, in this context, Hh acts through a secondary signal, Bmp4, to pattern myogenic mesenchyme in the developing small

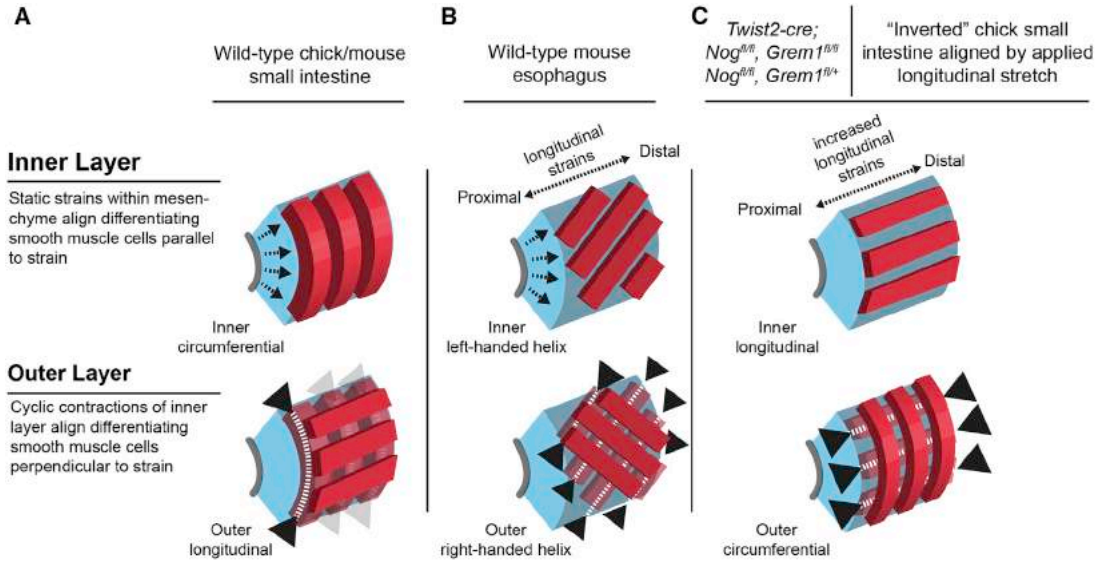

Figure 7. Model of Mechanically Controlled Smooth Muscle Alignment

(A) Residual strains in the mesenchyme lead to circumferential tensions that align differentiating muscle circumferentially. When formed, the cyclic contractions of the inner layer align the outer layer in the perpendicular, longitudinal direction.

(B) In the esophagus of mice, longitudinal tension and longitudinal residual strain are present in the mesenchyme and result in an inner left-handed helical array of muscle. Contractions of the inner layer cause the outer layer to align perpendicularly in a right-handed helix.

(C) When *Nog* is deleted from the mesoderm (along with one or two copies of *Grem1*), there is increased longitudinal strain in undifferentiated mesenchyme, and the inner layer aligns longitudinally. The longitudinal contractions of this layer align the outer layer circumferentially. This inversion of muscle layers is phenocopied by applying longitudinal stretch to the chick small intestine.

intestine. In the model presented here, Hh secreted by the endoderm activates Bmp4 at high concentrations in subepithelial mesenchyme, whereas Bmp2/7 are expressed in the outer mesothelium, generating a gradient of Bmp activity within the mesenchyme that results in a low-Bmp-activity sweet spot where the circumferential layer is specified to form and subsequently differentiates in a Hh-dependent manner. The integration of these signaling systems occurs at the level of myogenic transcription factors. Although Shh induces expression of *MYOCD*, Bmp signaling represses *MYOCD* and *MRTFA/B*.

Following formation of the inner layer of smooth muscle, secretion of Bmp antagonists by this layer itself and invading neural crest cells alters the morphogenic landscape, allowing differentiation of subsequent layers. Although the Hh-Bmp signaling axis determines the timing and location of muscle layer formation relative to the luminal and serosal surfaces of the gut tube, additional factors must be involved; for example, to sharpen and maintain the borders of each layer. One potential candidate is the Hippo pathway, which maintains the inner mesenchyme of the stomach in an undifferentiated state by repressing Hh-induced smooth muscle differentiation (Cotton et al., 2017). Whether components of the Hippo pathway are regulated by the Hh-Bmp axis or dependent on mechanical cues remains to be determined.

Multiple Roles of Signals in Gut Morphogenesis

In addition to the role we defined here in establishing smooth muscle pattern, the Hh-Bmp signaling axis is required for several other aspects of gut morphogenesis. Early on, it is critical for recruiting splanchnic mesoderm to surround the endoderm (Roberts et al., 1995). Then, as enteric neural crest cells migrate through the gut, Shh and Bmp signaling effect their movement and patterning (Goldstein et al., 2005; Nagy et al., 2016). At later stages, localized Hh signaling sets up the villus cluster signaling centers, inducing high levels of Bmp expression that feed back on the endoderm to inhibit proliferation and localize stem cells (Shyer et al., 2015; Walton et al., 2012, 2016). In the formation of other gut-derived organs, Shh downregulation is critical for budding of the pancreas (Apelqvist et al., 1997). Shh is an essential component of the network regulating lung branching morphogenesis (Pepicelli et al., 1998) and, together with Bmp signaling, is important for separation of the trachea and esophagus (Que et al., 2006). Remarkably, this Hh-Bmp signaling axis is sustained throughout development and remains present in the mature gut, where it acts to maintain epithelial-mesenchymal homeostasis and morphology through the regulation of stem cell dynamics in the intestinal crypt and subepithelial myofibroblast activity (He et al., 2004; Zacharias et al., 2011).

Common Pathways Control Muscle Differentiation in Tubular Organs

Many smooth muscle-invested organs besides the gut display the common signaling architecture of an epithelial layer expressing Hh ligands and a subepithelial mesenchyme expressing Bmp. For example, in the bladder, Hh activates *Bmp4* in the subepithelial mesenchyme, where it also appears to repress smooth muscle to generate a concentric pattern akin to the gut (Cheng et al., 2008; Liu et al., 2010; Tasian et al., 2010). Conversely, in

the ureter, Hh-dependent Bmp4 expression in periureteral mesenchyme promotes *Myocd* expression and acts to enhance smooth muscle differentiation (Caubit et al., 2008; Mamo et al., 2017; Yu et al., 2002), similar to its effect on mesenchymal stem cells *in vitro* (Lagna et al., 2007). The diverse responses of smooth muscle cells and their precursors to Bmp ligands require further investigation, but it is plausible that these observed tissue-specific effects could be explained through unique combinatorial Bmp ligand/receptor signaling (Antebi et al., 2017) or because Bmp can act through both canonical (Smad1/5/9) and noncanonical MAPK (mitogen-activated protein kinase)-mediated pathways to elicit varied responses in diverse contexts (Wang et al., 2014). Indeed, although we observe an initial gradient of pSmad1/5/9 within the mesenchyme that correlates with a low-Bmp zone for muscle differentiation, the gradient quickly becomes obscured (until later, when it is focally downregulated in the differentiating outer layer) and, in fact, becomes secondarily upregulated within the circular layer. Thus, Bmp signaling appears to function in a biphasic manner during intestinal smooth muscle patterning. Early on, Bmp downregulation is required for muscle specification, whereas later, when the layers have been patterned, Bmp signaling is needed for muscle cell maturation toward the contractile phenotype (Notarnicola et al., 2012; Sagnol et al., 2014). A temporal switch in Bmp function is reminiscent of its role in cardiac myogenesis, where transient downregulation of Bmp activity is required for specification, whereas upregulation later on is required for differentiation (Ladd et al., 1998; Yuasa et al., 2005).

A New Paradigm for Understanding the Development of Muscle Alignment through Mechanical Control

There is a growing recognition of the role of physical forces in embryonic morphogenesis. In the developing gut, physical forces regulate looping (Nerurkar et al., 2017; Savin et al., 2011), endodermal folding (Shyer et al., 2013), neural crest cell migration (Chevalier et al., 2016), and, as we show here, muscle layer orientation. Extensive *in vitro* and theoretical studies have demonstrated the effect of static and cyclic stretch on cell orientation (Buck, 1980; Faust et al., 2011; Kanda et al., 1992; Kim et al., 1999; Livne et al., 2014; Safran and De, 2009), but the *in vivo* use of these strains in aligning cells of developing tissues has remained unclear. We show that, in the gut, differential proliferation (growth) across the radial axis generates static strain to orient the first layer circumferentially, and cyclic contractions of this first layer subsequently align the second layer in a perpendicular orientation longitudinally. Why fibroblastic cells would respond in an orthogonal manner to cyclic versus static stretch is not intuitive. In the case where cells align parallel to a continuous stretch, it is because they act to reduce perceived strain (Eastwood et al., 1998). One plausible difference in the case of cyclic forces is that the cells are periodically contracted as well as periodically stretched, and the dominant response could be one of minimizing these strains. One model put forth to explain this reorientation response to cyclic stretch/compression suggests that cells avoid strain by aligning toward the angle of minimal substrate deformation (i.e., the direction of minimal strain) (Buck, 1982). This response is likely mediated through an initial realignment of stress fibers, which, through focal adhesions, anchor the cell to the substrate and together act to reorient the cell by relaxing its elastic energy to a minimum (Livne et al., 2014). Although one can thus provide models to rationalize the observed change in orientation, how a cell responds and aligns to strain likely depends on several variables, such as strain frequency, magnitude, cell type, and the physical and molecular properties of the ECM (extracellular matrix) substrate to which the cells are attached (Tamiello et al., 2016).

We have extended our studies from the circumferential and longitudinal muscles of the chick midgut to those of the mouse ureter and the helically wound muscles of the mouse esophagus to show evidence that this mechanism may be generally applicable in other tubular systems (Figures 7A–7C). The helical arrangement of esophageal muscle corresponds to the presence of longitudinal strains in the undifferentiated mesenchyme. How the handedness of the first muscle layer is determined is not clear, but we speculate that it might be due to dorsal/ventral asymmetries that arise during early foregut patterning perhaps because of the division of the trachea and esophagus. Along these lines, how the loss of Bmp antagonists within this mesenchyme results in enhanced longitudinal strain with the esophagus needs further investigation and might contribute to our understanding of how signaling pathways confer mechanical properties to these tissues.

A mechanical role of muscle in morphogenesis is well appreciated in the musculoskeletal system, where continuous tension drives myoblast fusion (Vandenburgh and Karlisch, 1989), spontaneous twitching enhances the formation of cross-striated muscle (Weitkunat et al., 2017), and muscle contraction is required for normal skeletal development (reviewed in Felsenthal and Zelzer, 2017). Here we demonstrated that the spontaneous contractions of one muscle layer can affect the alignment of a second layer, setting up a way to create multi-layered muscular tissues, determined by mechanical forces. This mechanism may act in concert with other mechanical cues, such as traction forces generated by fibroblasts (Stopak and Harris, 1982) or tension provided by tendons (Felsenthal and Zelzer, 2017), to aid in the alignment of skeletal muscle. Additionally, although we have demonstrated a clear cellular response to physical forces, our model does not necessarily preclude a role of the extracellular matrix, which itself can be aligned by mechanical stimuli and might act as a scaffold to aid and maintain cell alignment (Nam et al., 2016; Vader et al., 2009).

Mechanical forces can be sensed by cells in multiple ways (Chanet and Martin, 2014), and, ultimately, these forces must be interpreted by the cell and translated into modifications of the cytoskeleton and/or gene expression to achieve cellular alignment and tissue shape (Chanet et al., 2017). Only recently have potential genetic mediators of smooth muscle alignment been identified *in vivo*. For example, mouse mutants for *Wnt5a*, its receptor *Ror2*, and the ion channels *Kcnj13* and *Tmem16a* show misaligned smooth muscle in the mouse trachea and esophagus (Kishimoto et al., 2018; Rock et al., 2008; Yin et al., 2018), and mutations in the planar cell polarity (PCP) gene *Dlgh1* cause a misalignment of muscle in the mouse ureter (Mahoney et al., 2006). It is, however, currently unclear whether these genes modulate tissue mechanics to organize muscle or

whether their expression and cellular organization are downstream of mechanical cues, as demonstrated for PCP components within the mammalian skin (Aw et al., 2016). Further analyses of these and other genes in light of our findings will help clarify how smooth muscle cells and their precursors sense and respond to stresses and strains in the developing embryo.

Many hollow tubular organs are surrounded by layers of smooth muscle with specific orientations. Moreover, the pattern of stepwise differentiation and alignment of developing smooth muscle layers is common to other tubular systems, such as blood vessels (Greif et al., 2012) and organs of the urogenital tract (Georgas et al., 2015; Tasian et al., 2010; Viana et al., 2007), thus pointing to the possibility that the mechanism described above may act to align sequentially differentiating muscle in a variety of organs. The dependence of the second-forming muscle layer's alignment on the contractions of the first layer establishes a way to generate multi-layered smooth muscle with orthogonal alignments in tissues of diverse embryonic origin because cell alignment within a developing organ can be determined independent of the signaling environment and, instead, by generalizable physical parameters. Although it is currently not understood how the calcium-mediated spontaneous contractions first initiate in the embryonic gut, the fact that these early contractions are mechanosensitive (Chevalier, 2018) raises the possibility of a mechanical feedback, where the same tensile strain that orients the first muscle layer also acts to initiate its spontaneous contraction. In blood vessels, the pulsatile flow of luminal contents might act as another mechanical cue to guide vascular smooth muscle reorientation during development (Buck, 1980; Greif et al., 2012; Nandadasa et al., 2015). This physically guided mechanism of muscle alignment, in which the alignment of the first layer controls that of the second, might also be applicable across evolutionary scales because orthogonal muscle alignment is conserved in the guts of vertebrates and invertebrates as well as within the body plans of worms and hydra, where they play important roles in regeneration (Aghajanian et al., 2016; Brunet et al., 2016; Clark and Cowey, 1958; Livshits et al., 2017; Scimone et al., 2017; Seiler et al., 2010; Wallace and Burns, 2005). Indeed, there may be broad generality to the integrated mechanisms we described here, where the differentiation of a first-forming smooth muscle layer alters both the signaling and mechanical landscape of the primordial tissue and thereby sets the stage for proper morphogenesis of subsequently forming layers.

STAR★METHODS

Detailed methods are provided in the online version of this paper and include the following:

- KEY RESOURCES TABLE
- LEAD CONTACT AND MATERIALS AVAILABILITY
- EXPERIMENTAL MODEL AND SUBJECT DETAILS
  - Chickens
  - Mice
- METHOD DETAILS
  - Explant Cultures
  - Cut-open (flat) explants
  - Ureter explant cultures
  - Mouse esophagus explants
  - Uniaxial stretch experiments in cell culture
  - Whole gut explant uniaxial cyclic stretching
  - Whole gut static stretching
  - Whole mount immunostaining
  - Section immunostaining
  - Fluorescent *in situ* hybridization
  - Cell culture immunofluorescence
  - Imaging
  - Live imaging of calcium dynamics
  - CAM culture and neural crest ablation
  - Aphidicolin injection and EdU Labeling
  - Chick midgut electroporation
  - EdU/BrdU pulse labeling
  - Gene expression analysis (RT-qPCR)
- QUANTIFICATION AND STATISTICAL ANALYSIS
  - Quantification of smooth muscle orientation
  - Quantification of radial patterns in cross sections
  - Opening angle measurements
  - Esophageal strain measurements
  - Cell cycle length quantification from EdU/BrdU pulse labeling
  - Contraction frequency measurements
- DATA AND CODE AVAILABILITY

SUPPLEMENTAL INFORMATION

Supplemental Information can be found online at https://doi.org/10.1016/j.cell.2019.08.041.

ACKNOWLEDGMENTS

We are grateful to Joe Patrice for providing excellent care for animals used in this study. We are additionally thankful to the members of the Tabin and Cepko labs, Maxwell Heiman, Olivier Pourquié, and David Breault, for thoughtful discussions of the work. We additionally thank the Microscopy Resources on the North Quad (MicRoN) core at Harvard Medical School. This work was funded by NIH F31DK111059 (to T.R.H.) and R01HD087234 (to C.J.T.).

AUTHOR CONTRIBUTIONS

T.R.H. and C.J.T. conceived the study. T.R.H. designed the experiments with additional contributions from N.L.N., L.M., and C.J.T. T.R.H. conducted the experiments for the ureter studies with contributions from B.M.M. H.K.G. and D.S. wrote the scripts for image quantification and radial pattern analysis. T.R.H. wrote and prepared the manuscript with assistance from C.J.T. and N.L.N. and input from all authors.

DECLARATION OF INTERESTS

The authors declare no competing interests.

Received: December 11, 2018
Revised: May 31, 2019
Accepted: August 22, 2019
Published: September 19, 2019

REFERENCES

Abzhanov, A., Protas, M., Grant, B.R., Grant, P.R., and Tabin, C.J. (2004). Bmp4 and morphological variation of beaks in Darwin's finches. Science *305*, 1462–1465.

Abzhanov, A., Rodda, S.J., McMahon, A.P., and Tabin, C.J. (2007). Regulation of skeletogenic differentiation in cranial dermal bone. Development *134*, 3133–3144.

Aghajanian, P., Takashima, S., Paul, M., Younossi-Hartenstein, A., and Hartenstein, V. (2016). Metamorphosis of the Drosophila visceral musculature and its role in intestinal morphogenesis and stem cell formation. Dev. Biol. *420*, 43–59.

Albinsson, S., Nordström, I., and Hellstrand, P. (2004). Stretch of the vascular wall induces smooth muscle differentiation by promoting actin polymerization. J. Biol. Chem. *279*, 34849–34855.

Amthor, H., Nicholas, G., McKinnell, I., Kemp, C.F., Sharma, M., Kambadur, R., and Patel, K. (2004). Follistatin complexes Myostatin and antagonises Myostatin-mediated inhibition of myogenesis. Dev. Biol. *270*, 19–30.

Antebi, Y.E., Linton, J.M., Klumpe, H., Bintu, B., Gong, M., Su, C., McCardell, R., and Elowitz, M.B. (2017). Combinatorial Signal Perception in the BMP Pathway. Cell *170*, 1184–1196.e24.

Apelqvist, A., Ahlgren, U., and Edlund, H. (1997). Sonic hedgehog directs specialised mesoderm differentiation in the intestine and pancreas. Curr. Biol. *7*, 801–804.

Aw, W.Y., Heck, B.W., Joyce, B., and Devenport, D. (2016). Transient Tissue-Scale Deformation Coordinates Alignment of Planar Cell Polarity Junctions in the Mammalian Skin. Curr. Biol. *26*, 2090–2100.

Barlow, A.J., Wallace, A.S., Thapar, N., and Burns, A.J. (2008). Critical numbers of neural crest cells are required in the pathways from the neural tube to the foregut to ensure complete enteric nervous system formation. Development *135*, 1681–1691.

Bitgood, M.J., and McMahon, A.P. (1995). Hedgehog and Bmp genes are coexpressed at many diverse sites of cell-cell interaction in the mouse embryo. Dev. Biol. *172*, 126–138.

Bono, N., Pezzoli, D., Levesque, L., Loy, C., Candiani, G., Fiore, G.B., and Mantovani, D. (2016). Unraveling the role of mechanical stimulation on smooth muscle cells: A comparative study between 2D and 3D models. Biotechnol. Bioeng. *113*, 2254–2263.

Brunet, T., Fischer, A.H., Steinmetz, P.R., Lauri, A., Bertucci, P., and Arendt, D. (2016). The evolutionary origin of bilaterian smooth and striated myocytes. eLife *5*, e19607.

Buck, R.C. (1980). Reorientation response of cells to repeated stretch and recoil of the substratum. Exp. Cell Res. *127*, 470–474.

Buck, R.C. (1982). The influence of contact guidance on the orientation of colonies of subcultured vascular smooth muscle cells. In Vitro *18*, 783–788.

Capdevila, J., and Johnson, R.L. (1998). Endogenous and ectopic expression of noggin suggests a conserved mechanism for regulation of BMP function during limb and somite patterning. Dev. Biol. *197*, 205–217.

Capdevila, J., Tsukui, T., Rodríquez Esteban, C., Zappavigna, V., and Izpisúa Belmonte, J.C. (1999). Control of vertebrate limb outgrowth by the proximal factor Meis2 and distal antagonism of BMPs by Gremlin. Mol. Cell *4*, 839–849.

Caubit, X., Lye, C.M., Martin, E., Coré, N., Long, D.A., Vola, C., Jenkins, D., Garratt, A.N., Skaer, H., Woolf, A.S., and Fasano, L. (2008). Teashirt 3 is necessary for ureteral smooth muscle differentiation downstream of SHH and BMP4. Development *135*, 3301–3310.

Chanet, S., and Martin, A.C. (2014). Mechanical force sensing in tissues. Prog. Mol. Biol. Transl. Sci. *126*, 317–352.

Chanet, S., Miller, C.J., Vaishnav, E.D., Ermentrout, B., Davidson, L.A., and Martin, A.C. (2017). Actomyosin meshwork mechanosensing enables tissue shape to orient cell force. Nat. Commun. *8*, 15014.

Cheng, W., Yeung, C.K., Ng, Y.K., Zhang, J.R., Hui, C.C., and Kim, P.C. (2008). Sonic Hedgehog mediator Gli2 regulates bladder mesenchymal patterning. J. Urol. *180*, 1543–1550.

Chevalier, N.R. (2018). The first digestive movements in the embryo are mediated by mechanosensitive smooth muscle calcium waves. Philos. Trans. R. Soc. Lond. B Biol. Sci. *373*, 20170322.

Chevalier, N.R., Fleury, V., Dufour, S., Proux-Gillardeaux, V., and Asnacios, A. (2017). Emergence and development of gut motility in the chicken embryo. PLoS ONE *12*, e0172511.

Chevalier, N.R., Gazguez, E., Bidault, L., Guilbert, T., Vias, C., Vian, E., Watanabe, Y., Muller, L., Germain, S., Bondurand, N., et al. (2016). How Tissue Mechanical Properties Affect Enteric Neural Crest Cell Migration. Scientific reports *6*, 20927.

Clark, R.B., and Cowey, J.B. (1958). Factors Controlling the Change of Shape of Certain Nemertean and Turbellarian Worms. J. Exp. Biol. *35*, 731–748.

Coletta, R., Roberts, N.A., Randles, M.J., Morabito, A., and Woolf, A.S. (2018). Exogenous transforming growth factor-beta1 enhances smooth muscle differentiation in embryonic mouse jejunal explants. Journal of tissue engineering and regenerative medicine *12*, 252–264.

Cotton, J.L., Li, Q., Ma, L., Park, J.S., Wang, J., Ou, J., Zhu, L.J., Ip, Y.T., Johnson, R.L., and Mao, J. (2017). YAP/TAZ and Hedgehog Coordinate Growth and Patterning in Gastrointestinal Mesenchyme. Dev. Cell *43*, 35–47.e4.

Coulombre, A.J., and Coulombre, J.L. (1958). Intestinal development. I. Morphogenesis of the villi and musculature. J. Embryol. Exp. Morphol. *6*, 403–411.

De Santa Barbara, P., Williams, J., Goldstein, A.M., Doyle, A.M., Nielsen, C., Winfield, S., Faure, S., and Roberts, D.J. (2005). Bone morphogenetic protein signaling pathway plays multiple roles during gastrointestinal tract development. Dev. Dyn. *234*, 312–322.

Eastwood, M., Mudera, V.C., McGrouther, D.A., and Brown, R.A. (1998). Effect of precise mechanical loading on fibroblast populated collagen lattices: morphological changes. Cell Motil. Cytoskeleton *40*, 13–21.

Faust, U., Hampe, N., Rubner, W., Kirchgessner, N., Safran, S., Hoffmann, B., and Merkel, R. (2011). Cyclic stress at mHz frequencies aligns fibroblasts in direction of zero strain. PLoS ONE *6*, e28963.

Felsenthal, N., and Zelzer, E. (2017). Mechanical regulation of musculoskeletal system development. Development *144*, 4271–4283.

Francis, P.H., Richardson, M.K., Brickell, P.M., and Tickle, C. (1994). Bone morphogenetic proteins and a signalling pathway that controls patterning in the developing chick limb. Development *120*, 209–218.

Fung, Y.C. (1991). What are the residual stresses doing in our blood vessels? Ann. Biomed. Eng. *19*, 237–249.

Gazzerro, E., Smerdel-Ramoya, A., Zanotti, S., Stadmeyer, L., Durant, D., Economides, A.N., and Canalis, E. (2007). Conditional deletion of gremlin causes a transient increase in bone formation and bone mass. The Journal of biological chemistry *282*, 31549–31557.

Gabella, G. (2002). Development of visceral smooth muscle. Results Probl. Cell Differ. *38*, 1–37.

Georgas, K.M., Armstrong, J., Keast, J.R., Larkins, C.E., McHugh, K.M., Southard-Smith, E.M., Cohn, M.J., Batourina, E., Dan, H., Schneider, K., et al. (2015). An illustrated anatomical ontology of the developing mouse lower urogenital tract. Development *142*, 1893–1908.

Goldstein, A.M., Brewer, K.C., Doyle, A.M., Nagy, N., and Roberts, D.J. (2005). BMP signaling is necessary for neural crest cell migration and ganglion formation in the enteric nervous system. Mech. Dev. *122*, 821–833.

Greif, D.M., Kumar, M., Lighthouse, J.K., Hum, J., An, A., Ding, L., Red-Horse, K., Espinoza, F.H., Olson, L., Offermanns, S., and Krasnow, M.A. (2012). Radial construction of an arterial wall. Dev. Cell *23*, 482–493.

Hamburger, V., and Hamilton, H.L. (1992). A series of normal stages in the development of the chick embryo. 1951. Dev. Dyn. *195*, 231–272.

He, X.C., Zhang, J., Tong, W.G., Tawfik, O., Ross, J., Scoville, D.H., Tian, Q., Zeng, X., He, X., Wiedemann, L.M., et al. (2004). BMP signaling inhibits intestinal stem cell self-renewal through suppression of Wnt-beta-catenin signaling. Nat. Genet. *36*, 1117–1121.

Houston, B., Thorp, B.H., and Burt, D.W. (1994). Molecular cloning and expression of bone morphogenetic protein-7 in the chick epiphyseal growth plate. J. Mol. Endocrinol. *13*, 289–301.

Huang, H., Cotton, J.L., Wang, Y., Rajurkar, M., Zhu, L.J., Lewis, B.C., and Mao, J. (2013). Specific requirement of Gli transcription factors in Hedgehog-mediated intestinal development. J. Biol. Chem. *288*, 17589–17596.

Kan, A., Ikeda, T., Fukai, A., Nakagawa, T., Nakamura, K., Chung, U.I., Kawaguchi, H., and Tabin, C.J. (2013). SOX11 contributes to the regulation of GDF5 in joint maintenance. BMC Dev. Biol. *13*, 4.

Kanda, K., and Matsuda, T. (1994). Mechanical stress-induced orientation and ultrastructural change of smooth muscle cells cultured in three-dimensional collagen lattices. Cell Transplant. *3*, 481–492.

Kanda, K., Matsuda, T., and Oka, T. (1992). Two-dimensional orientational response of smooth muscle cells to cyclic stretching. ASAIO J. *38*, M382–M385.

Kedinger, M., Simon-Assmann, P., Bouziges, F., Arnold, C., Alexandra, E., and Haffen, K. (1990). Smooth muscle actin expression during rat gut development and induction in fetal skin fibroblastic cells associated with intestinal embryonic epithelium. Differentiation *43*, 87–97.

Kim, B.S., Nikolovski, J., Bonadio, J., and Mooney, D.J. (1999). Cyclic mechanical strain regulates the development of engineered smooth muscle tissue. Nat. Biotechnol. *17*, 979–983.

Kishimoto, K., Tamura, M., Nishita, M., Minami, Y., Yamaoka, A., Abe, T., Shigeta, M., and Morimoto, M. (2018). Synchronized mesenchymal cell polarization and differentiation shape the formation of the murine trachea and esophagus. Nat. Commun. *9*, 2816.

Kolterud, A., Grosse, A.S., Zacharias, W.J., Walton, K.D., Kretovich, K.E., Madison, B.B., Waghray, M., Ferris, J.E., Hu, C., Merchant, J.L., et al. (2009). Paracrine Hedgehog signaling in stomach and intestine: new roles for hedgehog in gastrointestinal patterning. Gastroenterology *137*, 618–628.

Ladd, A.N., Yatskievych, T.A., and Antin, P.B. (1998). Regulation of avian cardiac myogenesis by activin/TGFbeta and bone morphogenetic proteins. Dev. Biol. *204*, 407–419.

Lagna, G., Ku, M.M., Nguyen, P.H., Neuman, N.A., Davis, B.N., and Hata, A. (2007). Control of phenotypic plasticity of smooth muscle cells by bone morphogenetic protein signaling through the myocardin-related transcription factors. J. Biol. Chem. *282*, 37244–37255.

Lassar, A.B., Paterson, B.M., and Weintraub, H. (1986). Transfection of a DNA locus that mediates the conversion of 10T1/2 fibroblasts to myoblasts. Cell *47*, 649–656.

Lecoin, L., Gabella, G., and Le Douarin, N. (1996). Origin of the c-kit-positive interstitial cells in the avian bowel. Development *122*, 725–733.

Lewis, A.E., Vasudevan, H.N., O'Neill, A.K., Soriano, P., and Bush, J.O. (2013). The widely used Wnt1-Cre transgene causes developmental phenotypes by ectopic activation of Wnt signaling. Dev. Biol. *379*, 229–234.

Li, A., Cho, J.H., Reid, B., Tseng, C.C., He, L., Tan, P., Yeh, C.Y., Wu, P., Li, Y., Widelitz, R.B., et al. (2018). Calcium oscillations coordinate feather mesenchymal cell movement by SHH dependent modulation of gap junction networks. Nat. Commun. *9*, 5377.

Liboska, R., Ligasová, A., Strunin, D., Rosenberg, I., and Koberna, K. (2012). Most anti-BrdU antibodies react with 2′-deoxy-5-ethynyluridine – the method for the effective suppression of this cross-reactivity. PLoS ONE *7*, e51679.

Liu, B., Feng, D., Lin, G., Cao, M., Kan, Y.W., Cunha, G.R., and Baskin, L.S. (2010). Signalling molecules involved in mouse bladder smooth muscle cellular differentiation. Int. J. Dev. Biol. *54*, 175–180.

Livne, A., Bouchbinder, E., and Geiger, B. (2014). Cell reorientation under cyclic stretching. Nat. Commun. *5*, 3938.

Livshits, A., Shani-Zerbib, L., Maroudas-Sacks, Y., Braun, E., and Keren, K. (2017). Structural Inheritance of the Actin Cytoskeletal Organization Determines the Body Axis in Regenerating Hydra. Cell Rep. *18*, 1410–1421.

Mahoney, Z.X., Sammut, B., Xavier, R.J., Cunningham, J., Go, G., Brim, K.L., Stappenbeck, T.S., Miner, J.H., and Swat, W. (2006). Discs-large homolog 1 regulates smooth muscle orientation in the mouse ureter. Proc. Natl. Acad. Sci. USA *103*, 19872–19877.

Mamo, T.M., Wittern, A.B., Kleppa, M.J., Bohnenpoll, T., Weiss, A.C., and Kispert, A. (2017). BMP4 uses several different effector pathways to regulate proliferation and differentiation in the epithelial and mesenchymal tissue compartments of the developing mouse ureter. Hum. Mol. Genet. *26*, 3553–3563.

Mao, J., Kim, B.M., Rajurkar, M., Shivdasani, R.A., and McMahon, A.P. (2010). Hedgehog signaling controls mesenchymal growth in the developing mammalian digestive tract. Development *137*, 1721–1729.

Marigo, V., and Tabin, C.J. (1996). Regulation of patched by sonic hedgehog in the developing neural tube. Proc. Natl. Acad. Sci. USA *93*, 9346–9351.

Martynoga, B., Morrison, H., Price, D.J., and Mason, J.O. (2005). Foxg1 is required for specification of ventral telencephalon and region-specific regulation of dorsal telencephalic precursor proliferation and apoptosis. Dev. Biol. *283*, 113–127.

McHugh, K.M. (1995). Molecular analysis of smooth muscle development in the mouse. Dev. Dyn. *204*, 278–290.

McMahon, J.A., Takada, S., Zimmerman, L.B., Fan, C.M., Harland, R.M., and McMahon, A.P. (1998). Noggin-mediated antagonism of BMP signaling is required for growth and patterning of the neural tube and somite. Genes Dev. *12*, 1438–1452.

Muzumdar, M.D., Tasic, B., Miyamichi, K., Li, L., and Luo, L. (2007). A global double-fluorescent Cre reporter mouse. Genesis *45*, 593–605.

Nagy, N., Barad, C., Graham, H.K., Hotta, R., Cheng, L.S., Fejszak, N., and Goldstein, A.M. (2016). Sonic hedgehog controls enteric nervous system development by patterning the extracellular matrix. Development *143*, 264–275.

Nam, E., Lee, W.C., and Takeuchi, S. (2016). Formation of Highly Aligned Collagen Nanofibers by Continuous Cyclic Stretch of a Collagen Hydrogel Sheet. Macromol. Biosci. *16*, 995–1000.

Nandadasa, S., Nelson, C.M., and Apte, S.S. (2015). ADAMTS9-Mediated Extracellular Matrix Dynamics Regulates Umbilical Cord Vascular Smooth Muscle Differentiation and Rotation. Cell Rep. *11*, 1519–1528.

Nerurkar, N.L., Mahadevan, L., and Tabin, C.J. (2017). BMP signaling controls buckling forces to modulate looping morphogenesis of the gut. Proc. Natl. Acad. Sci. USA *114*, 2277–2282.

Notarnicola, C., Rouleau, C., Le Guen, L., Virsolvy, A., Richard, S., Faure, S., and De Santa Barbara, P. (2012). The RNA-binding protein RBPMS2 regulates development of gastrointestinal smooth muscle. Gastroenterology *143*, 687–697.e9.

Orsulic, S., Li, Y., Soslow, R.A., Vitale-Cross, L.A., Gutkind, J.S., and Varmus, H.E. (2002). Induction of ovarian cancer by defined multiple genetic changes in a mouse model system. Cancer Cell *1*, 53–62.

Pepicelli, C.V., Lewis, P.M., and McMahon, A.P. (1998). Sonic hedgehog regulates branching morphogenesis in the mammalian lung. Curr. Biol. *8*, 1083–1086.

Que, J., Choi, M., Ziel, J.W., Klingensmith, J., and Hogan, B.L. (2006). Morphogenesis of the trachea and esophagus: current players and new roles for noggin and Bmps. Differentiation *74*, 422–437.

Ramalho-Santos, M., Melton, D.A., and McMahon, A.P. (2000). Hedgehog signals regulate multiple aspects of gastrointestinal development. Development *127*, 2763–2772.

Rens, E.G., and Merks, R.M.H. (2017). Cell Contractility Facilitates Alignment of Cells and Tissues to Static Uniaxial Stretch. Biophys. J. *112*, 755–766.

Rezakhaniha, R., Agianniotis, A., Schrauwen, J.T., Griffa, A., Sage, D., Bouten, C.V., van de Vosse, F.N., Unser, M., and Stergiopulos, N. (2012). Experimental investigation of collagen waviness and orientation in the arterial adventitia using confocal laser scanning microscopy. Biomech. Model. Mechanobiol. *11*, 461–473.

Riddle, R.D., Johnson, R.L., Laufer, E., and Tabin, C. (1993). Sonic hedgehog mediates the polarizing activity of the ZPA. Cell *75*, 1401–1416.

Roberts, D.J., Johnson, R.L., Burke, A.C., Nelson, C.E., Morgan, B.A., and Tabin, C. (1995). Sonic hedgehog is an endodermal signal inducing Bmp-4 and Hox genes during induction and regionalization of the chick hindgut. Development *121*, 3163–3174.

Roberts, D.J., Smith, D.M., Goff, D.J., and Tabin, C.J. (1998). Epithelial-mesenchymal signaling during the regionalization of the chick gut. Development *125*, 2791–2801.

Roberts, R.R., Ellis, M., Gwynne, R.M., Bergner, A.J., Lewis, M.D., Beckett, E.A., Bornstein, J.C., and Young, H.M. (2010). The first intestinal motility patterns in fetal mice are not mediated by neurons or interstitial cells of Cajal. J. Physiol. *588*, 1153–1169.

Rock, J.R., Futtner, C.R., and Harfe, B.D. (2008). The transmembrane protein TMEM16A is required for normal development of the murine trachea. Dev. Biol. *321*, 141–149.

Safran, S.A., and De, R. (2009). Nonlinear dynamics of cell orientation. Phys. Rev. E Stat. Nonlin. Soft Matter Phys. *80*, 060901.

Sagnol, S., Yang, Y., Bessin, Y., Allemand, F., Hapkova, I., Notarnicola, C., Guichou, J.F., Faure, S., Labesse, G., and de Santa Barbara, P. (2014). Homodimerization of RBPMS2 through a new RRM-interaction motif is necessary to control smooth muscle plasticity. Nucleic Acids Res. *42*, 10173–10184.

Savin, T., Kurpios, N.A., Shyer, A.E., Florescu, P., Liang, H., Mahadevan, L., and Tabin, C.J. (2011). On the growth and form of the gut. Nature *476*, 57–62.

Schneider, C.A., Rasband, W.S., and Eliceiri, K.W. (2012). NIH Image to ImageJ: 25 years of image analysis. Nat. Methods *9*, 671–675.

Schultz, T., Daniel, V., and Daniel, E.E. (2003). Does ICC pacing require functional gap junctions between ICC and smooth muscle in mouse intestine? Neurogastroenterol. Motil. *15*, 129–138.

Scimone, M.L., Cote, L.E., and Reddien, P.W. (2017). Orthogonal muscle fibres have different instructive roles in planarian regeneration. Nature *551*, 623–628.

Seiler, C., Abrams, J., and Pack, M. (2010). Characterization of zebrafish intestinal smooth muscle development using a novel sm22α-b promoter. Dev. Dyn. *239*, 2806–2812.

Shyer, A.E., Tallinen, T., Nerurkar, N.L., Wei, Z., Gil, E.S., Kaplan, D.L., Tabin, C.J., and Mahadevan, L. (2013). Villification: how the gut gets its villi. Science *342*, 212–218.

Shyer, A.E., Huycke, T.R., Lee, C., Mahadevan, L., and Tabin, C.J. (2015). Bending gradients: how the intestinal stem cell gets its home. Cell *161*, 569–580.

Smith, D.M., Nielsen, C., Tabin, C.J., and Roberts, D.J. (2000). Roles of BMP signaling and Nkx2.5 in patterning at the chick midgut-foregut boundary. Development *127*, 3671–3681.

Southwell, B.R. (2006). Staging of intestinal development in the chick embryo. Anat. Rec. A Discov. Mol. Cell. Evol. Biol. *288*, 909–920.

Stafford, D.A., Brunet, L.J., Khokha, M.K., Economides, A.N., and Harland, R.M. (2011). Cooperative activity of noggin and gremlin 1 in axial skeleton development. Development *138*, 1005–1014.

Stopak, D., and Harris, A.K. (1982). Connective tissue morphogenesis by fibroblast traction. I. Tissue culture observations. Dev. Biol. *90*, 383–398.

Streit, A., Lee, K.J., Woo, I., Roberts, C., Jessell, T.M., and Stern, C.D. (1998). Chordin regulates primitive streak development and the stability of induced neural cells, but is not sufficient for neural induction in the chick embryo. Development *125*, 507–519.

Sukegawa, A., Narita, T., Kameda, T., Saitoh, K., Nohno, T., Iba, H., Yasugi, S., and Fukuda, K. (2000). The concentric structure of the developing gut is regulated by Sonic hedgehog derived from endodermal epithelium. Development *127*, 1971–1980.

Tamiello, C., Buskermolen, A.B.C., Baaijens, F.P.T., Broers, J.L.V., and Bouten, C.V.C. (2016). Heading in the Right Direction: Understanding Cellular Orientation Responses to Complex Biophysical Environments. Cell. Mol. Bioeng. *9*, 12–37.

Tasian, G., Cunha, G., and Baskin, L. (2010). Smooth muscle differentiation and patterning in the urinary bladder. Differentiation *80*, 106–117.

Vader, D., Kabla, A., Weitz, D., and Mahadevan, L. (2009). Strain-induced alignment in collagen gels. PLoS ONE *4*, e5902.

Vandenburgh, H.H., and Karlisch, P. (1989). Longitudinal growth of skeletal myotubes in vitro in a new horizontal mechanical cell stimulator. In Vitro Cell. Dev. Biol., *25*, pp. 607–616.

Viana, R., Batourina, E., Huang, H., Dressler, G.R., Kobayashi, A., Behringer, R.R., Shapiro, E., Hensle, T., Lambert, S., and Mendelsohn, C. (2007). The development of the bladder trigone, the center of the anti-reflux mechanism. Development *134*, 3763–3769.

Visel, A., Thaller, C., and Eichele, G. (2004). GenePaint.org: an atlas of gene expression patterns in the mouse embryo. Nucleic Acids Res. *32*, D552–D556.

Wallace, A.S., and Burns, A.J. (2005). Development of the enteric nervous system, smooth muscle and interstitial cells of Cajal in the human gastrointestinal tract. Cell Tissue Res. *319*, 367–382.

Walton, K.D., Kolterud, A., Czerwinski, M.J., Bell, M.J., Prakash, A., Kushwaha, J., Grosse, A.S., Schnell, S., and Gumucio, D.L. (2012). Hedgehog-responsive mesenchymal clusters direct patterning and emergence of intestinal villi. Proc. Natl. Acad. Sci. USA *109*, 15817–15822.

Walton, K.D., Whidden, M., Kolterud, Å., Shoffner, S.K., Czerwinski, M.J., Kushwaha, J., Parmar, N., Chandhrasekhar, D., Freddo, A.M., Schnell, S., and Gumucio, D.L. (2016). Villification in the mouse: Bmp signals control intestinal villus patterning. Development *143*, 427–436.

Wang, Z., Wang, D.-Z., Pipes, G.C.T., and Olson, E.N. (2003). Myocardin is a master regulator of smooth muscle gene expression. Proc. Natl. Acad. Sci. USA *100*, 7129–7134.

Wang, R.N., Green, J., Wang, Z., Deng, Y., Qiao, M., Peabody, M., Zhang, Q., Ye, J., Yan, Z., Denduluri, S., et al. (2014). Bone Morphogenetic Protein (BMP) signaling in development and human diseases. Genes Dis. *1*, 87–105.

Weidenhamer, N.K., and Tranquillo, R.T. (2013). Influence of cyclic mechanical stretch and tissue constraints on cellular and collagen alignment in fibroblast-derived cell sheets. Tissue Eng. Part C Methods *19*, 386–395.

Weitkunat, M., Brasse, M., Bausch, A.R., and Schnorrer, F. (2017). Mechanical tension and spontaneous muscle twitching precede the formation of cross-striated muscle *in vivo*. Development *144*, 1261–1272.

Yin, W., Kim, H.T., Wang, S., Gunawan, F., Wang, L., Kishimoto, K., Zhong, H., Roman, D., Preussner, J., Guenther, S., et al. (2018). The potassium channel KCNJ13 is essential for smooth muscle cytoskeletal organization during mouse tracheal tubulogenesis. Nat. Commun. *9*, 2815.

Yu, J., Carroll, T.J., and McMahon, A.P. (2002). Sonic hedgehog regulates proliferation and differentiation of mesenchymal cells in the mouse metanephric kidney. Development *129*, 5301–5312.

Yu, K., Xu, J., Liu, Z., Sosic, D., Shao, J., Olson, E.N., Towler, D.A., and Ornitz, D.M. (2003). Conditional inactivation of FGF receptor 2 reveals an essential role for FGF signaling in the regulation of osteoblast function and bone growth. Development *130*, 3063–3074.

Yuasa, S., Itabashi, Y., Koshimizu, U., Tanaka, T., Sugimura, K., Kinoshita, M., Hattori, F., Fukami, S., Shimazaki, T., Ogawa, S., et al. (2005). Transient inhibition of BMP signaling by Noggin induces cardiomyocyte differentiation of mouse embryonic stem cells. Nat. Biotechnol. *23*, 607–611.

Zacharias, W.J., Madison, B.B., Kretovich, K.E., Walton, K.D., Richards, N., Udager, A.M., Li, X., and Gumucio, D.L. (2011). Hedgehog signaling controls homeostasis of adult intestinal smooth muscle. Dev. Biol. *355*, 152–162.

STAR★METHODS

KEY RESOURCES TABLE

REAGENT or RESOURCE	SOURCE	IDENTIFIER
Antibodies		
Mouse Anti-alpha smooth muscle Actin antibody (Clone 1A4) (FITC-conjugated)	Abcam	Cat#ab8211; RRID:AB_306359
Mouse Anti-alpha smooth muscle Actin antibody (Clone 1A4) (Cy3-conjugated)	Sigma	Cat#C6198; RRID:AB_476856
Rabbit Anti-Phospho-Smad1 (Ser463/465)/ Smad5 (Ser463/465)/ Smad9 (Ser465/467) (Clone D5B10)	Cell Signaling Technologies	Cat#13820; RRID:AB_2493181
Rabbit Anti-beta III Tubulin antibody	Abcam	Cat#ab18207; RRID:AB_444319
Rabbit Anti-TAGLN/Transgelin antibody	Abcam	Cat#ab14106; RRID:AB_443021
Rabbit Anti-phospho-Histone H3 (Ser10)	Sigma	Cat#06-570; RRID:AB_310177
Mouse Anti-RCAS (gag-pro)	DSHB	Cat#AMV-3C2; RRID:AB_528098
Mouse Anti-BrdU (Clone MoBU-1)	ThermoFisher	Cat#B35128; RRID:AB_2536432
Rabbit Anti-Calponin 1 (Clone D8L2T)	Cell Signaling Technologies	Cat#17819; RRID:AB_2798789
Rabbit Anti-smooth muscle Myosin heavy chain 11	Abcam	Cat#ab53219; RRID:AB_2147146
Alexa Fluor® 488 AffiniPure Donkey Anti-Mouse IgG (H+L)	Jackson ImmunoResearch	Cat#715-545-150; RRID:AB_2340846
Alexa Fluor® 647 AffiniPure Donkey Anti-Rabbit IgG (H+L)	Jackson ImmunoResearch	Cat#711-605-152; RRID:AB_2492288
Cy3 AffiniPure Donkey Anti-Rabbit IgG (H+L)	Jackson ImmunoResearch	Cat#711-165-152; RRID:AB_2307443
Alexa Fluor® 488 AffiniPure Donkey Anti-Rabbit IgG (H+L)	Jackson ImmunoResearch	Cat#711-545-152; RRID:AB_2313584
Cy3 AffiniPure Donkey Anti-Mouse IgG (H+L)	Jackson ImmunoResearch	Cat#715-165-150; RRID:AB_2340813
Alexa Fluor® 647 AffiniPure Donkey Anti-Mouse IgG (H+L)	Jackson ImmunoResearch	Cat#715-605-150; RRID:AB_2340862
Biotin-SP (long spacer) AffiniPure Goat Anti-Rabbit IgG (H+L)	Jackson ImmunoResearch	Cat#111-065-003; RRID:AB_2337959
Peroxidase Streptavidin	Jackson ImmunoResearch	Cat#016-030-084; RRID:AB_2337238
Chemicals, Peptides, and Recombinant Proteins		
Recombinant Mouse Sonic Hedgehog/Shh (C25II) N terminus	R&D Systems	Cat#464-SH
Recombinant Mouse BMP-4 Protein	R&D Systems	Cat#5020-BP
Recombinant Mouse Noggin (aa 28-232) Protein	R&D Systems	Cat#6997-NG
Recombinant Human TGF-beta 1 Protein	R&D Systems	Cat#240-B
Cyclopamine	Millipore	Cat#239803
Smoothened Agonist	Millipore	Cat#566660
Dorsomorphin dihydrochloride	Tocris	Cat#3093
LDN 193189 hydrochloride	Abcam	Cat#ab142186
Nifedipine	Sigma	Cat#N7634
ML-7 hydrochloride	Tocris	Cat#4310
Carbenoxolone disodium	Tocris	Cat#3096
(S)-(-)-Bay K 8644	Tocris	Cat#1546
Aphidicolin	Tocris	Cat#5736
Critical Commercial Assays		
Click-iT EdU Alexa Fluor Imaging Kit	ThermoFisher	Cat#C10337
SuperScript III First-Strand Synthesis System	ThermoFisher	Cat#18080051
AzuraQuant Green Fast qPCR Mix LoRox	Azura Genomics	Cat#AZ-2105

(*Continued on next page*)

Continued

REAGENT or RESOURCE	SOURCE	IDENTIFIER
Experimental Models: Organisms/Strains		
*Mouse: Noggin$^{fl/fl}$: **N**og$^{tm1.1Rmh}$/J*	Jackson Laboratory (Stafford et al., 2011)	JAX: 016117
Mouse: Gremlin1$^{fl/fl}$	Gazzerro et al., 2007	N/A
Mouse: Twist2-cre (Dermo-cre): B6.129X1-*Twist2*$^{tm1.1(cre)Dor}$/J	Jackson Laboratory (Yu et al., 2003)	JAX: 008712
Mouse: Wnt1-Cre: B6.Cg-*E2f1*$^{Tg(Wnt1-cre)2Sor}$/J	Jackson Laboratory (Lewis et al., 2013)	JAX: 022501
Mouse: mT/mG: B6.129(Cg)-*Gt(ROSA)26Sor*$^{tm4(ACTB-tdTomato,-EGFP)Luo}$/J	Jackson Laboratory (Muzumdar et al., 2007)	JAX: 007676
Mouse: C57BL/6J	Jackson Laboratory	JAX: 000664
Oligonucleotides		
Primers for RT-qPCR, see Table S1	This paper	N/A
Primers for Genotyping, see Table S1	This paper	N/A
Primers for ISH probe generation, see Table S1	This paper	N/A
Recombinant DNA		
Chick PTCH1 probe	Marigo and Tabin, 1996	N/A
Chick BMP4 probe	Francis et al., 1994	N/A
Chick BMP2 probe	Francis et al., 1994	N/A
Chick BMP7 probe	Houston et al., 1994	N/A
Chick NOGGIN probe	Capdevila and Johnson, 1998	N/A
Chick GREM1 probe	Capdevila et al., 1999	N/A
Chick FST probe	Amthor et al., 2004	N/A
Chick CHRD probe	Streit et al., 1998	N/A
Mouse Noggin probe	McMahon et al., 1998	N/A
RCAS-Shh	Riddle et al., 1993	Addgene Plasmid #13991
RCAS-Noggin	Abzhanov et al., 2004	N/A
RCAS-GFP	Kan et al., 2013	Addgene Plasmid #13878
RCAS-Bmp2	Nerurkar et al., 2017	N/A
RCAS-GCaMP6s-T2A-mCherry	Li et al., 2018	N/A
RCAS-myrAKT	Orsulic et al., 2002	Addgene Plasmid #11547
RCAS-Myc	Orsulic et al., 2002	Addgene Plasmid #11548
Software and Algorithms		
ImageJ	NIH	https://imagej.nih.gov/ij/
Graphpad Prism 8	Graphpad	https://www.graphpad.com/scientific-software/prism/
MATLAB	Mathworks	https://www.mathworks.com/products/matlab.html
Radial Pattern Quantification (MATLAB)	This Paper	https://github.com/dsprinzak/huycke-et-al-Cell-2019
Other		
Alexa Fluor 647 Phalloidin	ThermoFisher	Cat#A22287
StrexCell Cell Stretching System	STREX	Model#STB-140-04

LEAD CONTACT AND MATERIALS AVAILABILITY

Further information and requests for resources and reagents should be directed to and will be fulfilled by the Lead Contact, Clifford Tabin (tabin@genetics.med.harvard.edu).

EXPERIMENTAL MODEL AND SUBJECT DETAILS

All animal studies were performed in compliance with NIH guidelines and standard operating protocols approved by the Institutional Animal Care and Use Committee at Harvard Medical School.

Chickens

Fertilized Specific Pathogen Free (SPF) White Leghorn Chicken eggs (Charles River) were incubated in a 38°C humidified chamber with embryos staged according to Hamburger and Hamilton (1992) and guts to Southwell (2006).

Mice

Mouse lines in this study were previously described: mice harboring floxed *Noggin* (Stafford et al., 2011) and floxed *Gremlin1* (Gazzerro et al., 2007) were a gift from Richard Harland (UC Berkeley), and *Twist2-cre* (Yu et al., 2003), *Wnt1-cre* (Lewis et al., 2013) and ROSA$^{mT/mG}$ (Muzumdar et al., 2007) mice were obtained from JAX (stocks #008712, #022501, #007676). *Twist2-cre* mice were crossed with *Wnt1-cre* to generate mice containing both Cre genes. These in turn were bred to mice homozygous for both *Nog* and *Grem1* conditional alleles. The resultant mice hemizygous for all alleles were thus maintained on a mixed FVB, C57BL/6J background and crossed to homozygous floxed mice to generate embryos at desired stages for experimentation. For esophageal measurements, *Twist2-cre* mice were crossed to *Nog* and *Grem1* floxed mutants and bred in a similar manner. Each Cre line was crossed to ROSA$^{mT/mG}$ reporter mice to confirm activity. Mice were PCR genotyped with primers listed in the above original references or on the JAX website (Table S1). Controls analyzed for small intestine smooth muscle development were mice with both Cre drivers but hemizygous for the floxed alleles (*Twist2-cre, Wnt1-cre; Nog*$^{fl/+}$*, Grem1*$^{fl/+}$) or mice lacking Cre but homozygous for both floxed alleles (*Nog*$^{fl/fl}$*, Grem1*$^{fl/fl}$), neither of which had any notable phenotypes when compared with to standard wild-type C57BL/6J mice. For experiments involving the ureter, timed pregnant CD-1 mice (Charles River) were used.

METHOD DETAILS

Explant Cultures

All chick explants were cultured in DMEM containing 1% Pen/Strep and 10% chick embryo extract (U.S. Biological). All mouse explants were cultured in DMEM containing 1% Pen/Strep and 10% FBS. These tissues were grown in a humidified 37°C incubator with 5% CO_2. For experiments in which explants were incubated with pharmacological compounds, the following stock solutions were used and diluted in culture media to final concentrations listed in figures: Recombinant mouse N-Shh (500μM in PBS +0.1% BSA, R&D Systems), mouse Bmp4 (100μg/mL in 4mM HCl and 0.1% BSA, R&D Systems), mouse Noggin (100μg/mL in PBS + 0.1% BSA, R&D Systems), cyclopamine (2.5mM in ethanol, Millipore), aphidicolin (10mg/mL in DMSO, Tocris), LDN-193189 hydrochloride (10mM in water, Sigma), dorsomorphin dihydrochloride (10mM in water, Tocris), nifedipine (200mM in DMSO, Sigma), ML-7 (50mM in DMSO, Tocris), carbenoxolone (100mM in water, Tocris), (S)-(-)-Bay K 8644 (100mM in DMSO, Tocris). In all experiments, equivalent amounts of vehicle were added to control explants. Unless otherwise noted, media changes were performed every 24 hours. For the Shh soaked bead experiment, a Heparin bead (Sigma) was soaked in 10mg/mL recombinant Shh on ice for 1 hour before being implanted into the gut mesoderm. For standard chick experiments, whole guts were dissected and explants were pinned to 5% agarose beds in 12 or 24 well dishes at the early stages (E4-6) with 0.002 inch or 0.004 inch diameter tungsten rods (A-M systems), which were pierced through the gizzard and hindgut. Guts were held taught, but not stretched, and positioned along the pins near the surface of the culture media to enhance gas exchanged. Later stage explants (chick E9-12, except stretch experiments detailed below) were cultured on 0.4μm PTFE membrane inserts (Millicell) at the air-liquid interphase in 6 well dishes. For those cultured on membranes, 1.8mL culture media was used as this amount was enough to maintain the sample morphology (so as to not become flattened against the membrane) while at the same time preventing the tissue from free floating, which impairs morphogenesis. All mouse gut explants were carried out with the latter method on PTFE membrane inserts. For E9 chick cultures, standard chick explant media was supplemented with 1ng/mL human recombinant TGFβ1 (R&D Systems) to enhance the frequency of explants that developed longitudinal smooth muscle for analysis as previously described (Coletta et al., 2018). Explants were cultured with 2-3 guts per well.

Cut-open (flat) explants

Whole midgut segments were dissected from the embryo at stages defined in figures. A tungsten rod (either 0.002 inch diameter or 0.004 inch diameter was used depending on stage) was used to pierce the lumen of the tube, and fine forceps were used to cut along the length of one side of the intubated tube, causing it to open up. During the culture period, the explants naturally flatten out due to the faster growth rate of the inner layers relative to the outer layers. Flattened explants were cultured on PTFE membrane inserts, except for experiments when stretch was applied, and in which case the guts were cultured pinned to agarose. Guts were grown with lumen facing up or down, but no differences were noted in experimental outcome.

Ureter explant cultures

Mouse ureters were dissected from embryos from timed pregnant CD-1 mice (Charles River) at E16.5 and placed on 0.4μm PTFE culture inserts (Millicell) in 6 well plates, with 4 ureters to a well. Ureters were cultured in DMEM supplemented with 10% FBS and

1% Penicillin/Streptomycin. For nifedipine treated ureters, nifedipine (Sigma) was resuspended in DMSO to 200mM and added to the media at 50μM. Ureters were cultured for 72 hours at 37°C with daily media changes.

Mouse esophagus explants

Whole E12.5 mouse digestive tracts were dissected away from the embryo and cultured on 0.4μm PTFE culture inserts (Millicell) in 6 well plates. Media was changed once at 36 hours during a 72 hour culture period. Nifedipine and ML-7 were dissolved in DMSO to final concentrations of 60μM (nifedipine) and 45μM (ML-7) to inhibit contractions. Foreguts were cultured either with or without the developing airway attached to the esophagus, though we noted no difference between the two conditions.

Uniaxial stretch experiments in cell culture

E12 chick midguts were dissected from the embryo in cold PBS before being transferred to a solution of 1% trypsin in DMEM and placed in a 37°C incubator. After 20 minutes, the endodermal epithelium and serosal mesothelium had begun to shed and were mechanically separated from the mesenchyme with fine forceps. Following 10 more minutes of incubation at 37°C, FBS was added to the media to a final concentration of 10% and the cells were dissociated via rapid pipetting with a 25 gauge syringe. The suspension was filtered twice through a 70μm strainer, after which cells were seeded at 4x10^5 density on PDMS chambers (STREX) coated with Fibronectin (Sigma, 0.05mg/mL at 37°C for 2 hours). Cells cultured in DMEM supplemented with 1% Pen/Strep and 10% Chick Embryo Extract (US Biological) were allowed to adhere overnight, and following a media change the adhered cells were subjected to either 20% static stretch or 15% cyclic stretch at a frequency of 1Hz for 96 hours in the STB-140 Strex cell stretching system (STREX) housed within an incubator at 37°C and 5% CO_2. Media was changed every 48 hours.

Whole gut explant uniaxial cyclic stretching

For cyclic stretch experiments, whole midguts from E9 chick embryos were dissected in cold PBS and mesentery was removed. Midguts were transferred to warm chick explant culture media (DMEM containing 1% Pen/Strep, 10% Chick embryo extract), separated into jejunal and ileal halves by bisecting the midgut at the attachment point of the superior mesenteric artery, though we noted no differences between the segments in their responses to cyclic stretch. Segments were then carefully transferred again into a 1.0 × 0.6 × 1.0 cm PDMS stretch chamber (STREX #STB-CH-0.06) filled with culture media so that the well itself was overflowing and a thin film of media spread across the top of the chamber. The explants were then pinned to the PDMS on either side of the well with 0.002 inch diameter tungsten rods pierced through the gut such that the midgut segments were held taught, but not stretched, across the well and along the long axis of the chamber (for longitudinal stretching). Up to 3 midguts were placed in a single chamber, and the chambers were subsequently placed in the Strex cell stretching system, which was used to apply 15% uniaxial cyclic stretch at a frequency of 10 cycles (sine wave) per minute (0.1667 Hz) for 72 hours in an incubator at 37°C and 5% CO_2. To prevent media evaporation, several dishes of DI water were placed within the Strex system and additionally a pipette tip box top was placed over the stretching chambers. Approximately every 12 hours the tungsten rods were repositioned to keep the gut segments taught as otherwise slack would build between the two pinned points (due to growth and the viscoelasticity of the gut) and stretch would no longer be applied. Media was added dropwise to each chamber at these 12 hour time points to ensure the tissue did not dry out. The media was completely replaced at 36 hours. Nifedipine was dissolved in DMSO to 200mM and used at a final concentration of 100μM. These experiments were additionally repeated essentially the same as above but with the addition of 0.005 inch diameter tungsten rods inserted through the lumen to intubate the guts and prevent transverse compression. Briefly, the midguts segments were excised from the embryo, and the tungsten rod was threaded through the lumen of each segment with care as not to damage the endoderm or perforate the gut wall. Rods were cut such that the midgut segments maintained non-intubated regions at the ends that could be used to pin the segments to the PDMS stretch chamber as above.

Whole gut static stretching

Static stretch was applied to chick midgut segments in culture by pinning explants to the well of a 12 well plate filled with 5% agarose in DMEM. Explants were pinned using a 0.004 inch tungsten rod to pierce through the gizzard (stomach) and hindgut, with stretch being applied longitudinally across the length of the midgut. Approximately 20% stretch was achieved by first removing the mesentery and pinning the gut taught (but unstretched) to the agarose bed, measuring the length of the midgut segment between the pins, and then removing one of the pins and placing it at an increased distance to change the length and thus stretch the midgut by about 20% of its original length. Additional 20% longitudinal stretch was reapplied in the same manner by increasing the distance between the pins every 24 hours to maintain the strained state. Media was replaced every 36 hours. For experiments to generate inverted smooth muscle alignment in Figure 4E, guts were grown an additional 96 hours following the period of continuous stretch by placing the pins closer together and thus relieving the strain.

Whole mount immunostaining

Whole, freshly dissected or cultured guts and ureters were fixed in 4% formaldehyde overnight at 4°C. Tissues were washed twice briefly with PBS and permeabilized for at least 2 hours with PBS containing 0.1% Triton X-100 and 0.05% Tween-20. Tissues were then blocked for 1 hour with PBS/1%BSA and then incubated with primary antibodies at 4°C overnight. The following day, tissues

were rinsed 3 times with PBS and subsequently incubated with secondary antibodies overnight at 4°C. Following several PBS washes, tissues were mounted in glass bottom fluorodishes (World Precision Instruments) for imaging.

Section immunostaining

Tissues were fixed in 4% formaldehyde at 4°C overnight while straightened and pinned to agarose, washed twice with PBS, and then dehydrated in 30% sucrose/PBS overnight at 4°C. The sucrose solution was then replaced with OCT twice, before mounting the tissue in blocks, paying careful attention to maintain straight tissue alignment. Transverse cryosections were obtained at 14μm, allowed to dry for 30 minutes, and either stained immediately or stored at −80°C. Immunostaining was performed identically to the whole-mount protocol listed above. Staining was performed with the following primary antibodies: αSMA-cy3 (1:500, C6198 Sigma), αSMA-FITC (1:500, F3777 Sigma), phospho-histone H3 (1:300, 06-570 Millipore), phospho-Smad1/5/9 (1:300, 13820S Cell Signaling Technology), β-III Tubulin (1:1000, ab18207 Abcam), Tagln (1:300, ab14106 Abcam), AMV-3C2 (1:100, DSHB). Species-specific secondary antibodies conjugated to fluorophores (Jackson Immuno) were used at 1:300. Phospho-Smad 1/5/9 staining was performed as previously described with a 5 minute pH6 citrate buffer antigen retrieval and signal amplification using a biotinylated secondary antibody (1:300, Jackson Immuno) and streptavidin-conjugated HRP (1:300, Jackson Immuno) combined with standard TSA amplification protocol (Perkin Elmer) (Nerurkar et al., 2017).

Fluorescent *in situ* hybridization

Fluorescent *in situ* hybridization was performed using standard protocols in combination with the TSA amplification kit (Perkin Elmer). Sections were rinsed 2 X 5 minutes with PBT (1X PBS and 0.1%Tween-20) and permeabilized with 1μg/mL Proteinase K for 10 minutes, followed by 2 X 5 minute PBT rinses and post-fixation with 4% formaldehyde/PBS for 5 minutes. After 4 X 5 minute additional PBT washes, probes were added in hybridization buffer to the slides and plastic coverslips were placed on the slides for hybridization overnight at 65°C in a humidified chamber. The next day slides were rinsed quickly in 5X SSC to remove the plastic coverslips, and stringency washes were as follows at 65°C: 1X SSC/ 50% formamide for 30 minutes, 2X SSC for 20 minutes, 0.2X SSC for 20 minutes twice. Slides were then rinsed 2 X 5 minutes in TNT (0.1 M Tris-HCl pH 7.5; 0.15 M NaCl; 0.05% Tween20) and peroxidase activity quenched with 3%H_2O_2 for 15 minutes. After rinsing 3 X 5 minutes with TNT, sections were blocked with TNTB blocking solution (Perkin Elmer) for 1 hour and replaced with 1:300 Anti-DIG-POD (Roche) overnight at 4°C. Following antibody labeling, unbound antibody was rinsed off with 4 X 5 minute TNT washes and TSA amplification was performed by adding Tyr-Cy3 or Tyr-Cy5 1:50 in amplification diluent to the slides for 7 minutes. After additional washes with TNT, slides were then incubated with additional primary antibodies using the standard immunostaining protocol above or stained with DAPI. DIG labeled probes were generated by *in vitro* transcription from either linearized plasmids (see Key Resources Table) or purified PCR products generated with primers containing a T3 promoter sequence on the 3′ primer (Table S1). Some mouse probes were generated using previous published primers from GenePaint (Visel et al., 2004; Table S1).

Cell culture immunofluorescence

Cells were fixed with 4% formaldehyde for 10 minutes at room temperature. Cells were then washed twice with PBS, permeabilized with PBSTT (PBS with 0.1% Triton X-100 and 0.05% Tween-20) for 20 minutes, and blocked with 1% BSA for 30 minutes. Cells were then incubated with primary antibody in PBS for 30 minutes at room temperature at concentrations listed above, followed by 3, 5 minute PBS washes before application of the secondary antibody for 30 minutes. All steps were performed on a shaker. PDMS wells (STREX) with stained cells were placed directly on coverslips for imaging.

Imaging

Images were captured on an inverted Zeiss LSM 710 confocal, Keyence BZ, or Leica stereoscope. Confocal imaging of whole mount samples was performed using a 40X water immersion lens on samples placed in glass bottom dishes (World Precision Instruments), while imaging of sections was performed at 63x or 10x depending on application. For high magnification acquisitions, images were acquired with pinhole set to approximately 1μm and a 1μm step size was used for Z stack collection. Maximum intensity projections of substacks specifically containing each layer were made using ImageJ (Schneider et al., 2012).

Live imaging of calcium dynamics

RCAS-GCaMP6S (Li et al., 2018) was electroporated into the lateral plate mesoderm at HH14 as described below. At specified times midguts were dissected from the embryo, and placed in 12 well PTFE membrane inserts placed within the bottom inset of glass bottom dishes (Matek) with a minimal amount of media consisting of Fluorobrite DMEM supplemented with 10% Chick Embryo Extract. Tissues were allowed to equilibrate for 6 hours in an incubator before imaging within a controlled incubator set to 37°C and 5% CO_2. Movies were taken at 1 frame per second.

CAM culture and neural crest ablation

Post umbilicus (yolk stalk) guts, in which neural crest cells had yet to migrate into, were dissected at E4 (HH23), comprising the ileum, ceca, and hindgut. The chorioallantoic membrane of a windowed, E8 host embryo was gently scratched with forceps to encourage vascularization following engraftment. Dissected guts were then transplanted onto the chorioallantoic membrane (CAM) of the host

and incubated for 8 days. Control guts were whole guts including the pre-umbilicus region in order to allow for neural crest cell migration. Following this period, successfully engrafted guts were dissected away from host tissue and kept on ice until further processing. For neural tube ablation, a pulled quartz needle was used to ablate the neural tube from somites 2-6 from embryos at stage HH10-12 as previously described (Barlow et al., 2008) to remove vagal neural crest cells that populate the gut and generate the enteric nervous system.

Aphidicolin injection and EdU Labeling

200μL of a 1mg/mL solution of Aphidicolin in PBS was injected into the amnion of a windowed chick egg at E4 via a 30 gauge syringe. The egg was then resealed and allowed to incubate for 2 days before tissue collection and fixation. For EdU labeling, 400μL of a 1mM EdU in PBS was injected via syringe into the amnion of the windowed chick embryo, which was allowed to incubate before the gut tissue was dissected and fixed for sectioning as described above. The Click-iT EdU (Invitrogen) reaction was carried out on sections as per manufacturer's instructions.

Chick midgut electroporation

Chick embryos were incubated to stage HH14-16, lowered, and windowed. Plasmids used for electroporation were previously described: RCAS-Shh (Riddle et al., 1993), RCAS-cmyc and RCAS-myrAkt (Orsulic et al., 2002), RCAS-Noggin (Abzhanov et al., 2004), RCAS-Bmp2 (Abzhanov et al., 2007), and RCAS-GCaMP6s-T2A-mCherry (Li et al., 2018). Plasmids were diluted to 2μg/μL in water with 0.1% fast green added to visualize DNA mix. This mix was injected via a pulled glass needle into the coelomic cavity on each side of the embryo that is situated between the lateral plate mesoderm compartments. Electrodes were place on either side of the embryo, with the positive located underneath and negative above, and electroporation was performed on a Nepa 21 electroporator (Nepa Gene) with the following parameters to drive the constructs into the splanchnic mesoderm: Poring pulse (voltage, 60V; pulse length, 5msec; pulse interval, 10msec; number of pulses, 5; decay, 0%; polarity, +) and Transfer pulse (voltage, 5V; pulse length, 10msec; pulse interval, 10msec; number of pulses, 5; decay, 0%; polarity, +/−). Tape was then placed over the windowed eggs, which were returned to incubation. After tissue processing as described above, high levels of infectivity were determined by 3C2 antibody staining, and only those with confirmed high levels (infectivity spread through the tissue) of staining were used for the study. Due to the timing of electroporation, the ileum of the midgut was mainly targeted and thus used for the majority of analyses. For controls, either mock electroporations or plasmids containing RCAS-GFP or mCherry were used. We noted no difference between any of the control conditions and non-electroporated/infected wild-type guts.

EdU/BrdU pulse labeling

Pulse labeling and cell quantification was performed based on a previously established paradigm (Martynoga et al., 2005). Chick eggs were windowed at E2.5 and electroporated as above. At E6.5, 500μl of a 1mM EdU solution in PBS was injected via syringe into the amniotic space adjacent to the developing gut. The eggs were then incubated for 1 hour and subsequently injected as above with a 10mM solution of BrdU in PBS and incubated an additional 30 minutes. As it takes approximately 30 minutes for the label to reach sufficiently detectable levels, the cells are able to incorporate EdU, but not BrdU, for a 1 hour period, and cells that are in the S-phase at the end of the experiment are labeled with BrdU. Guts were then dissected and fixed overnight at 4°C in 4% formaldehyde Whole mount immunostaining was performed as above with AMV-3C2 antibody to label identify electroporated/infected guts. These guts were then dehydrated in 30% sucrose for 2 hours at room temperature, then a 50/50 mix of 30% sucrose/OCT for an additional hour before being transferred to 100% OCT. Cryosectioning was performed to generate 10μm thick sections. Click-iT EdU labeling was performed with Alexa Fluor 647 per manufacturer's instructions (Invitrogen). Heat mediated antigen retrieval in pH6.0 10mM sodium citrate buffer was performed on the sections in a vegetable steamer for 15 minutes, and slides were then immediately removed and washed 3x5 minutes with PBS. Sections were then incubated with 1:100 anti-BrdU (MoBU-1, Invitrogen) in PBSTT, which has no cross-reactivity with EdU (Liboska et al., 2012), overnight at 4°C. Sections were then washed 4x5 minutes with PBS and incubated with a secondary anti-mouse Alexa Fluor 488 at 1:300 for 2 hours at room temperature.

Gene expression analysis (RT-qPCR)

RNA was isolated from guts using the RNeasy Micro Kit (QIAGEN), and cDNA was generated using Superscript III (ThermoFisher). Gene-specific primers were used to quantify gene expression via qPCR using AzuraQuant qPCR mix. Fold change expression was determined by the $2^{-\Delta\Delta CT}$ method with *GAPDH* as the reference gene. All experiments were performed with three biological replicates measured in triplicate. Primers are listed in Table S1.

QUANTIFICATION AND STATISTICAL ANALYSIS

Statistical analyses were performed using Prism 8 (GraphPad), and statistical details related to tests performed and sample size are specified in the figure legends.

Quantification of smooth muscle orientation

Quantification of smooth muscle orientation was performed using the distribution analysis function in the ImageJ plugin OrientationJ (Rezakhaniha et al., 2012) (Biomedical Imaging Group). 10μm thick substack maximum projections of Z-slices containing the cells of either the inner or outer layer were made from confocal Z stacks of whole mount guts stained with Smooth Muscle Actin. The enteric neural plexus (β-III Tubulin, SMA-negative) was used to distinguish between the location of inner and outer layers of muscle as these cells are situated specifically between the layers of muscle and can easily be distinguished due to their lack of SMA expression and DAPI staining in projections of the plexus. The distribution analysis function was run on the channel containing the SMA stain for a 100μm x 100μm region of interest (ROI), with a maximum of two separate, non-overlapping ROIs used for each image. For all midgut measurements, distribution angle values less than 0 were made positive so that all measurements were between 0 (longitudinal direction) and 90 (circumferential direction), whereas this step was not taken for esophageal alignment measurements in order to measure the pitch of the helically aligned muscle. Values for the histogram generated were normalized to the area under the curve (total distribution of orientations) to account for variations in staining between samples. Following normalization, the distribution for each orientation angle was averaged across a minimum of 10 ROIs per layer (obtained from at least 5 different experimental guts for each treatment) and plotted as a line graph.

Quantification of radial patterns in cross sections

Expression profiles were quantified using a custom image analysis pipeline in MATLAB. Multichannel images of gut transverse sections were manually segmented, where the outer boundary was drawn at the mesothelium, and the inner boundary was drawn at the basement membrane separating endoderm from mesenchyme. Segmented boundaries were used to generate a series of concentric rings of equal thickness in each radial direction. Mean fluorescence intensity was calculated within each ring and plotted against the center position of each ring along the radial axis. Distance of each position was calculated from the center of the lumen for images taken at 20X magnification, and from the endoderm for 63X images. For images where pSmad nuclear intensity was quantified, the DAPI channel was used to generate a mask that excluded all non-nuclear signal from intensity calculations. Replicate intensity profiles (derived from at least n = 4 images per treatment) were averaged after normalizing radial position with respect to the total radius between the inner and outer boundaries. Plots showing non-normalized radial position for individual replicates are shown in supplementary files. Images used for quantification were stained simultaneously and imaged with the same microscope settings.

Opening angle measurements

For radial opening angle measurements, tissues were dissected from the embryo and cut on a vibratome tissue chopper to generate 300μm segments. Using fine forceps and a pulled quartz needle while the gut segment was pinned through its lumen to agarose, a radial cut was made through the wall of the gut segment and allowed to relax for 5 minutes before images were taken on a Leica stereo dissecting scope. The opening angle was determined using ImageJ to find the angle between the two opened edges with the vertex in the center of the endoderm in the center of the opened tube as shown in Figure 3A. For longitudinal opening angle measurements, segments of esophageal tissue approximately 1mm in length were taken and a flame-sharpened 0.002 inch tungsten rod was used to pierce through the lumen while fine forceps were used to cut along the length until the tissue opened up. Tissue was allowed to relax 5 minutes before being imaged laterally, and the longitudinal opening angle was measured as the reflex angle from the original plane of the straight, unopened tube (180°).

For radial opening angle experiments on electroporated chick guts, following measurements of the opening angle, high levels of viral expression were confirmed via immunostaining for 3C2. Only samples that had high levels of 3C2 immunoreactivity (and thus high levels of infectivity) were used for quantification, as lower levels of viral expression did not result in a noticeable muscle alignment phenotype or changes to growth.

Esophageal strain measurements

Following timed matings, E12 mouse embryos were surgically opened with fine forceps with care being made not to disrupt the continuity of the gut from mouth to anus. Other visceral organs and connective tissue along with the developing airway was dissected away from the esophagus, all while leaving the entirety of the GI tract intact within the embryo. Then, using a glass capillary needle and mouth pipette DiI spots were placed along the length of the esophagus between its proximal end at the mouth and distal end at the stomach, and an image was taken to define the pre-cut state. Next, a cut was made at the proximal end of the esophagus near the connection to the mouth, and the esophagus was allowed to relax for 2 minutes before being imaged again to define the post-cut state. ImageJ was used to measure the distance between DiI spots discernable between the pre- and post-cut states, and the strain was measured as the difference between these two lengths divided by the post-cut length. Mutant embryos were pooled genotypes from 3 different crosses consisting of the following genotypes: *Twist2-cre; Nog*$^{fl/fl}$*, Grem1*$^{fl/fl}$, and *Twist2-cre; Nog*$^{fl/fl}$*, Grem1*$^{fl/+}$. All other possible genotype combinations from the crosses were littermates of the mutants pooled together as Controls except for *Twist2-cre; Nog*$^{fl/+}$*, Grem1*$^{fl/fl}$, which lacked an obvious phenotype but were omitted from the study.

Cell cycle length quantification from EdU/BrdU pulse labeling

S phase length and total cell cycle length was estimated using the technique in Martynoga et al., 2005. S-phase was calculated by the equation $Ts = Ti/(L_{cells}/S_{cells})$, where Ti is the duration cells can incorporate EdU but not BrdU (1 hour), L_{cells} is the fraction of cells that

are labeled with EdU only and have thus left the S phase during this period, and S_{cells} is the fraction that is labeled with BrdU. Total cell cycle length was calculated by the equation $Tc = Ts/(S_{cells}/P_{cells})$, where P_{cells} is the total number of dividing cells in the region of interest, which in the embryonic gut can be estimated by counting all cells. Two regions of interest were generated based on the location of the forming muscle layer for each section, and separate calculations were made for the inner mesenchyme and the muscle and outer mesenchyme together. Five guts were used for quantification per each treatment, with two sections used per gut such that a total of 10 sections were analyzed per treatment.

Contraction frequency measurements

Contraction frequency was measured by taking 2 minute movies of intestinal explants at 1 frame per second intervals on a Leica stereo microscope after 24-48 hours in culture and counting the number of contractions that occur over that time period at a particular point along the gut.

DATA AND CODE AVAILABILITY

The code for quantifying radial pattern generated in this study is available at GitHub (https://github.com/dsprinzak/huycke-et-al-Cell-2019).

Supplemental Figures

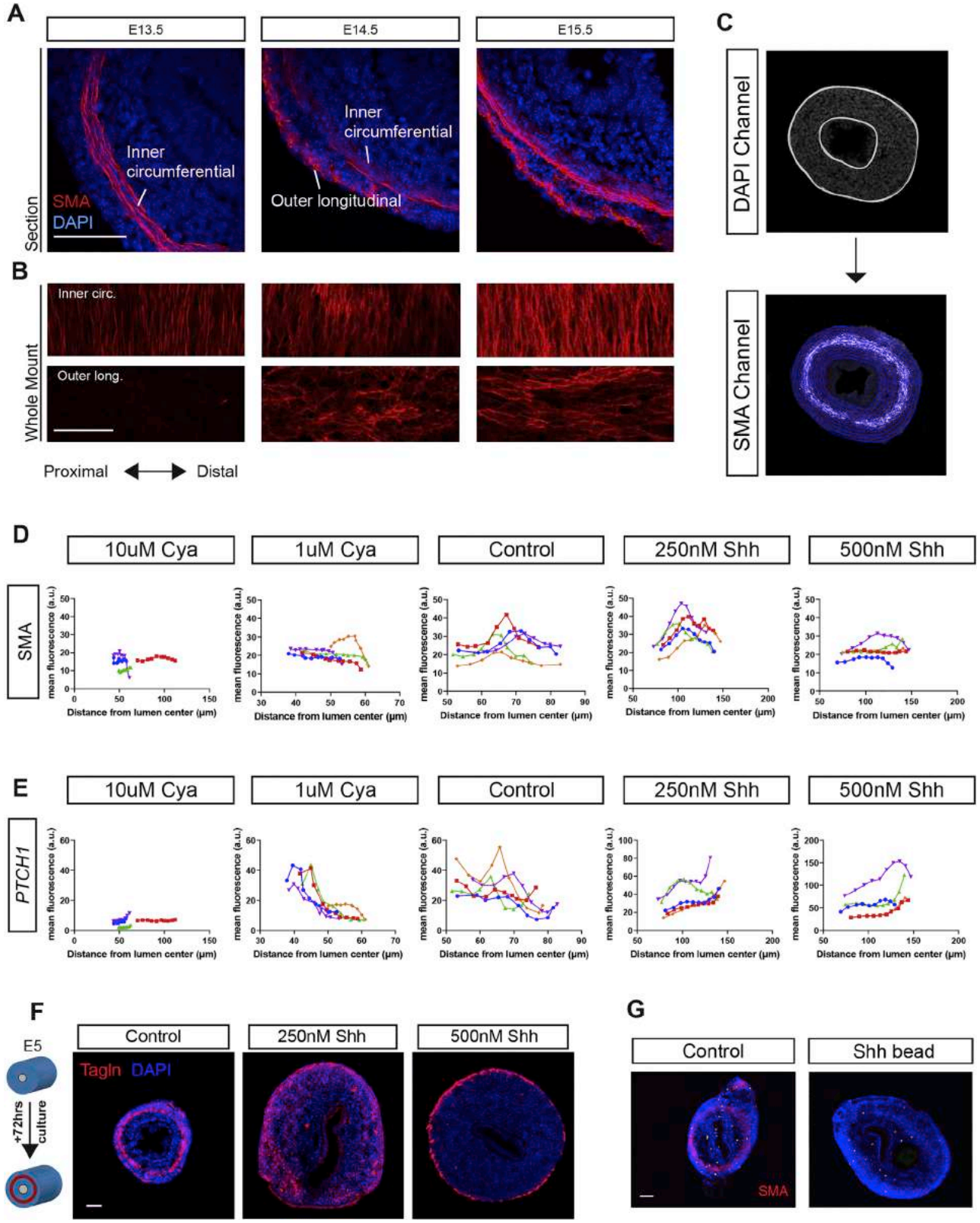

(legend on next page)

Figures S1. Hedgehog Signaling Patterns the Circumferential Muscle Layer, Related to Figures 1 and 3

(A) Transverse sections through the mouse jejunum stained with smooth muscle actin (SMA) and DAPI. (B) Whole-mount images of immunostained segments from equivalent stages as (A) during development demonstrating orthogonal alignment of layers.

(C) Demonstration of radial pattern quantification. (Top) DAPI channel of a transverse section used for segmentation. White lines indicate manually segmented boundaries at the inner endoderm and outer mesothelium. (Bottom) 10 concentric rings used to further segment a section into regions for intensity quantification (shown for example SMA channel). Blue lines specify the boundaries of each ring. For a given fluorescence signal, mean intensity within each ring is plotted against the central radial position between the ring boundaries for low magnification images of the whole gut, or plotted against the location of the basement membrane beneath the endoderm for high magnification partial gut images.

(D) Radial quantification data for SMA immunofluorescence used to generate plots in Figure 1, but shown with measured, unadjusted X (radial position) values. Each color represents an individual replicate

(E) Same as in (D) but with *PTCH1* FISH signal, corresponding to Figure 1.

(F) Sections from chick midgut explants treated with recombinant Shh and immunostained with the early smooth muscle marker Transgelin (Tagln, also known as Sm22α), which shows similar expression to αSMA.

(G) Shh-soaked bead implanted into mesenchyme inhibits smooth muscle differentiation.

Scale bars = 50μm.

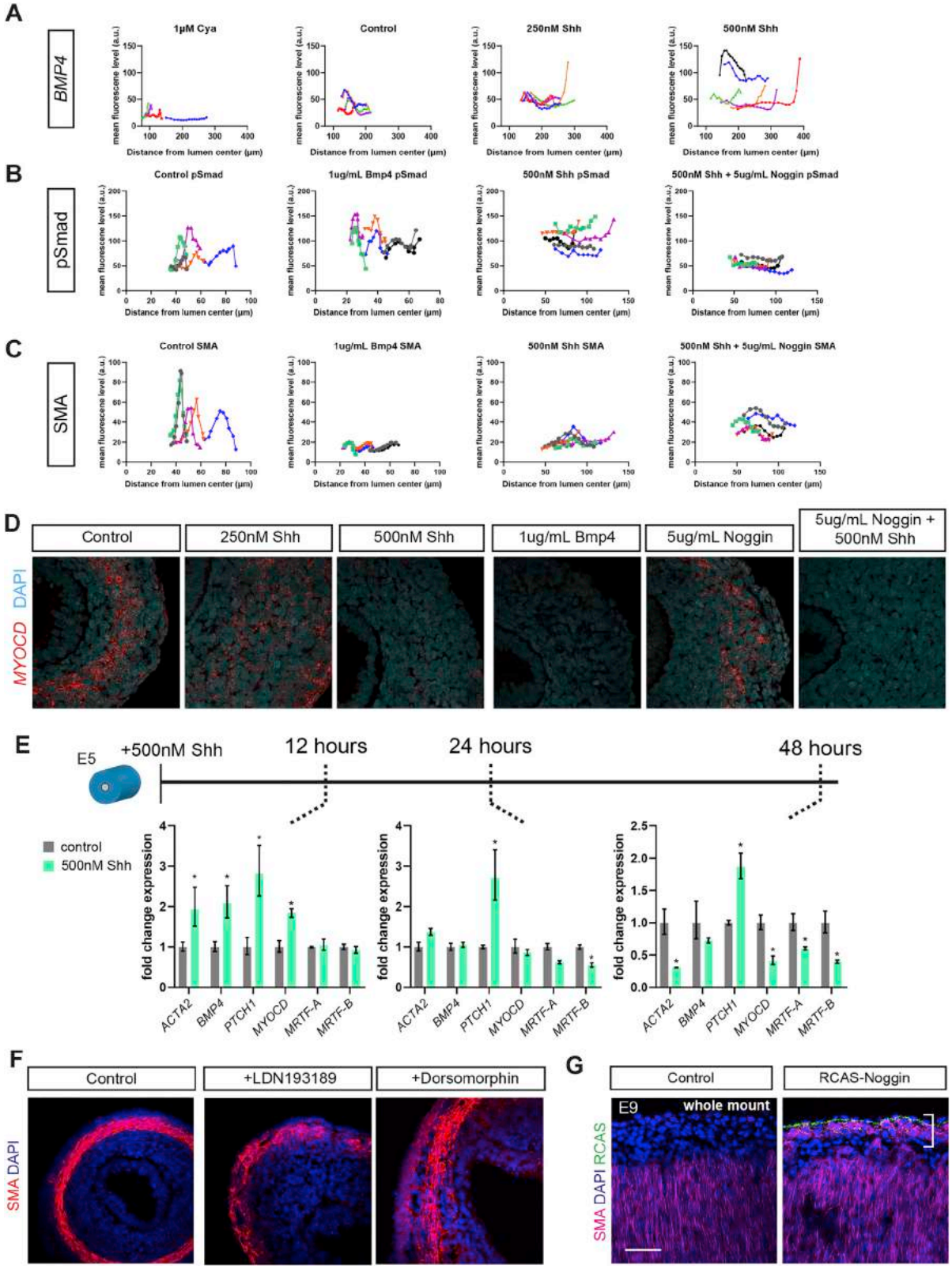

(legend on next page)

Figure S2. Hedgehog Signaling Acts through Bmp to Inhibit Smooth Muscle, Related to Figures 2 and 3

(A) Radial quantification data used to generate plot in Figure 2B, but shown with measured, unadjusted X (radial position) values. Each color represents an individual replicate.

(B) As in (A) but for pSmad1/5/9 staining in Figure 2D

(C) As in (A) but for αSMA staining in Figure 2D

(D) FISH for *MYOCARDIN* expression in chick explants treated for 72 hours with noted proteins. *MYOCD* is expressed in the presumptive smooth muscle layer, becoming more broadly expressed with the addition of 250nM Shh, but expression is lots with 500nM Shh or 1μg/mL Bmp4. Co-treatment of midgut explants with Noggin and the inhibitory dose of Shh induces smooth muscle throughout the mesenchyme, independently of *MYOCD*.

(E) RT-qPCR data during a 48 hour time course following incubation with 500nM recombinant Shh at E5 without media change. Three explanted midgut segments were taken out per treatment at the defined time points and used to quantify fold expression changes relative to *GAPDH*. The expression of muscle genes *MYOCD* and *ACTA2* initially increase, but not *MRTFA/B*, indicating that these are not Hh targets. Note that *BMP4* is only induced at the initial 12 hour time point, likely due to the fact that its induction requires high levels of Hh, which are no longer present in the media after 24 hours. By 48 hours, muscle gene repression is seen, including *MRTFA/B,* supporting that their repression requires *BMP4* induced by high Shh. Error bars are mean ± SD. *$p < 0.05$ by t test.

(F) Addition of Bmp antagonists LDN-193189 (2.5μM) and Dorsomorphin (5μM) in explant culture from E6 for 48 hours results in precocial outer layer differentiation as assessed by SMA immunofluorescence in outer mesenchyme adjacent to the mesothelium.

(G) RCAS-Noggin infected ileal segments display precocial smooth muscle in the outer layer compared to controls. Note the localized RCAS signal is likely due to the fact that electroporations performed in early lateral plate mesoderm tend to more effectively target tissues that become the outer mesenchyme.

Scale bars = 50μm.

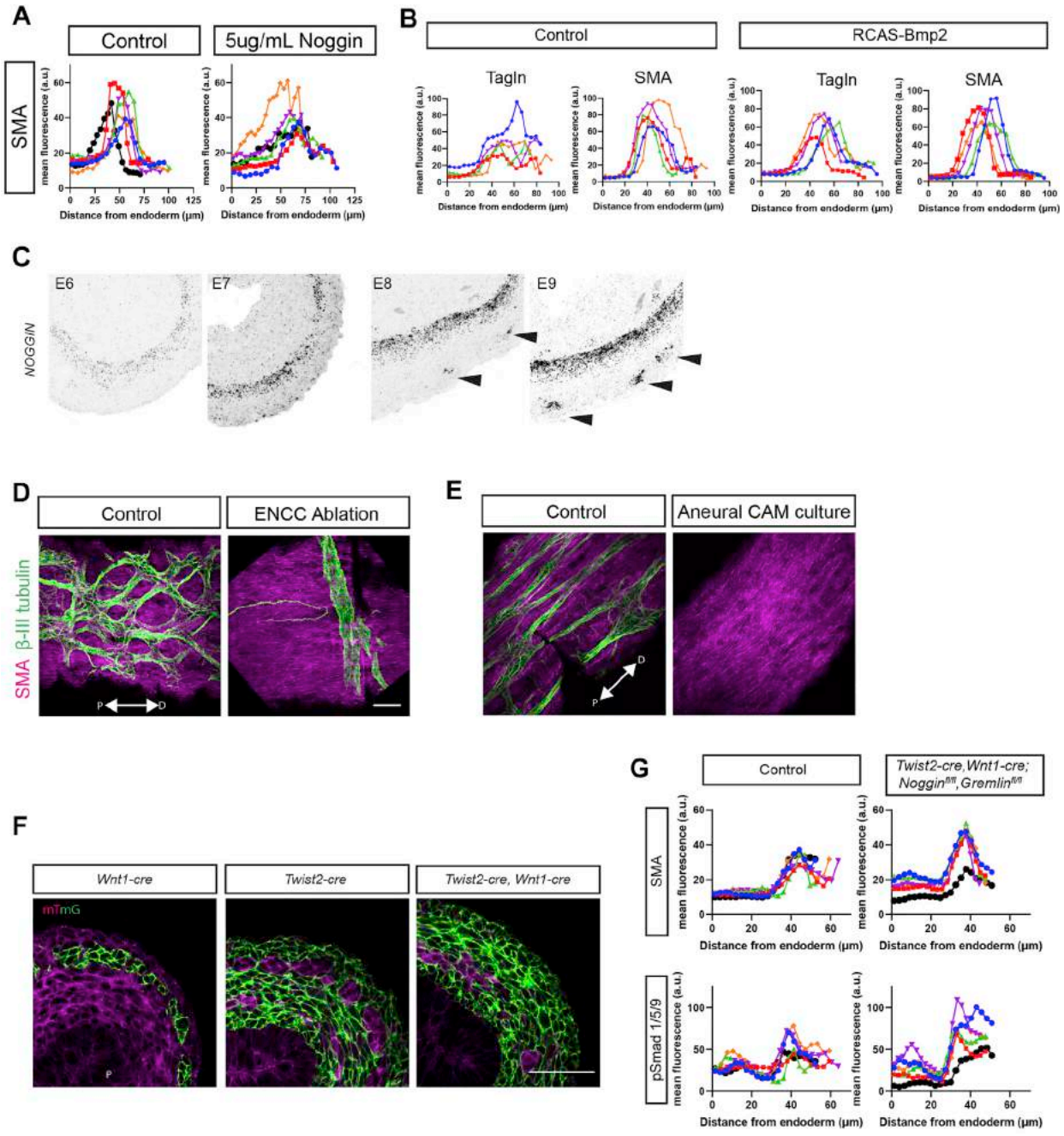

(legend on next page)

Figure S3. Bmp Signaling Regulates Outer Muscle Layer Formation, Related to Figure 3

(A) Radial quantification of SMA used to generate plots in Figure 3B, but with actual X values shown as distance from the endoderm. Each color represents an individual replicate.

(B) Radial quantification data of Tagln and SMA staining in cross sections used to generate plots in Figure 3E.

(C) FISH for *NOGGIN* expression in the chick midgut at stages prior to outer layer differentiation, demonstrating the expression in muscle becoming stronger over time and the emergence of expression within enteric neurons just prior to outer layer formation (black arrowheads).

(D) Whole mount of an E14 chick ileum from a midgut lacking enteric neural crest cells (ENCC) following their ablation at HH14. Note the axon present is extrinsic to the gut from the Nerve of Remak. Proximo-distal axis is noted.

(E) Whole mount of an aneural midgut grown on CAM cultured from E4 for 9 days.

(F) Sections from noted *Cre* mouse lines crossed with the ROSA$^{mT/mG}$ reporter. Sections are from jejunal segments at E13.5 showing *Cre* activity in green cells. Note the unlabeled cells in the dual *Cre* mouse are likely endothelial.

(G) Radial quantification data for SMA and pSmad1/5/9 used to generate plots in Figure 3G, showing each replicate and unadjusted X values.

(H) FISH for various Bmp pathway antagonists (yellow) during mouse and chick midgut development and immunostaining for SMA (magenta) to label muscle and β-III Tubulin (green) to label neurons. Sections are from jejunal segments at E13.5 (mouse) and E8 (chick), just prior to outer layer differentiation.

Scale bars = 50μm.

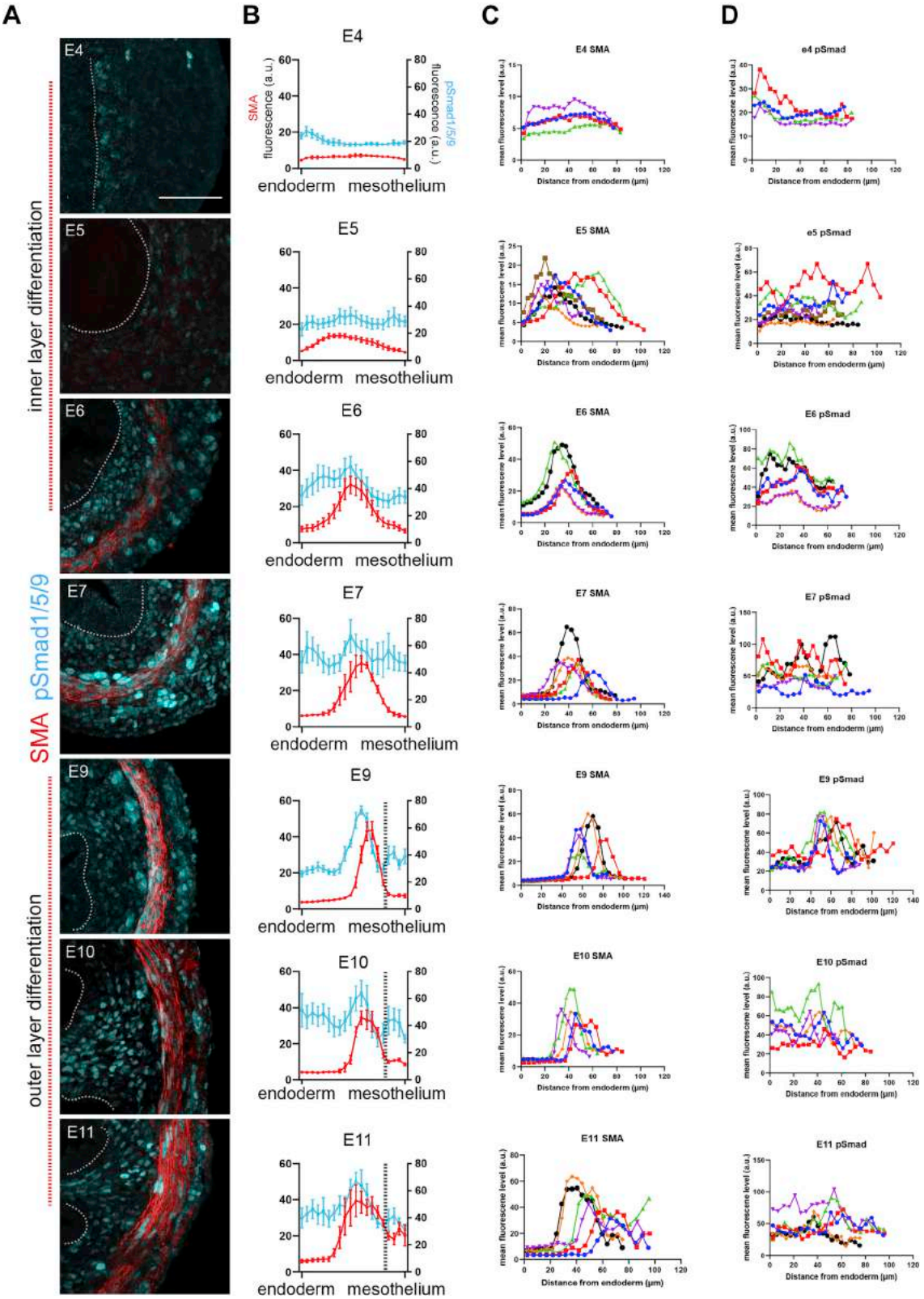

(legend on next page)

Figure S4. Canonical Bmp Signaling Dynamics during Intestinal Smooth Muscle Patterning, Related to Figures 2 and 3

(A) pSmad1/5/9 immunostaining of wild-type midgut sections showing Bmp signaling dynamics during muscle differentiation as assessed by SMA staining. Dashed white line denotes the endoderm-mesenchyme boundary.

(B) Quantification of radial pattern for SMA versus nuclear pSmad1/5/9 immunofluorescence in sections from (A). Nuclear pSmad1/5/9 is highest near the epithelium at E4 and forms a shallow gradient into the mesenchyme, mirroring the localized expression of *BMP4* within this same domain. Note that muscle differentiation, which begins to be apparent at E5, forms opposite the gradient at E4, and at this stage pSmad+ve cells are distributed throughout the mesenchyme, likely due to the emergence of an opposing gradient from the outer mesothelium. At E6, the inner edge of the differentiated muscle layer shows high Bmp signaling, indicative of its role in promoting smooth muscle maturation toward the contractile phenotype. At E7, both inner and outer mesenchyme have high levels of pSmad. Beginning at E9, pSmad levels begin to drop within the outer mesenchyme (indicated as the region to the right of the dashed line), correlating with the emergence of the outer muscle layer. Error bars are mean ± SEM.

(C) Radial quantification of SMA used to generate plots in (B) but with actual X values as distance from the endoderm. Each colored lines represents an individual replicate.

(D) Radial quantification of pSmad1/5/9 used to generate plots in (B) but with actual X values as distance from the endoderm.

Scale bars = 50μm.

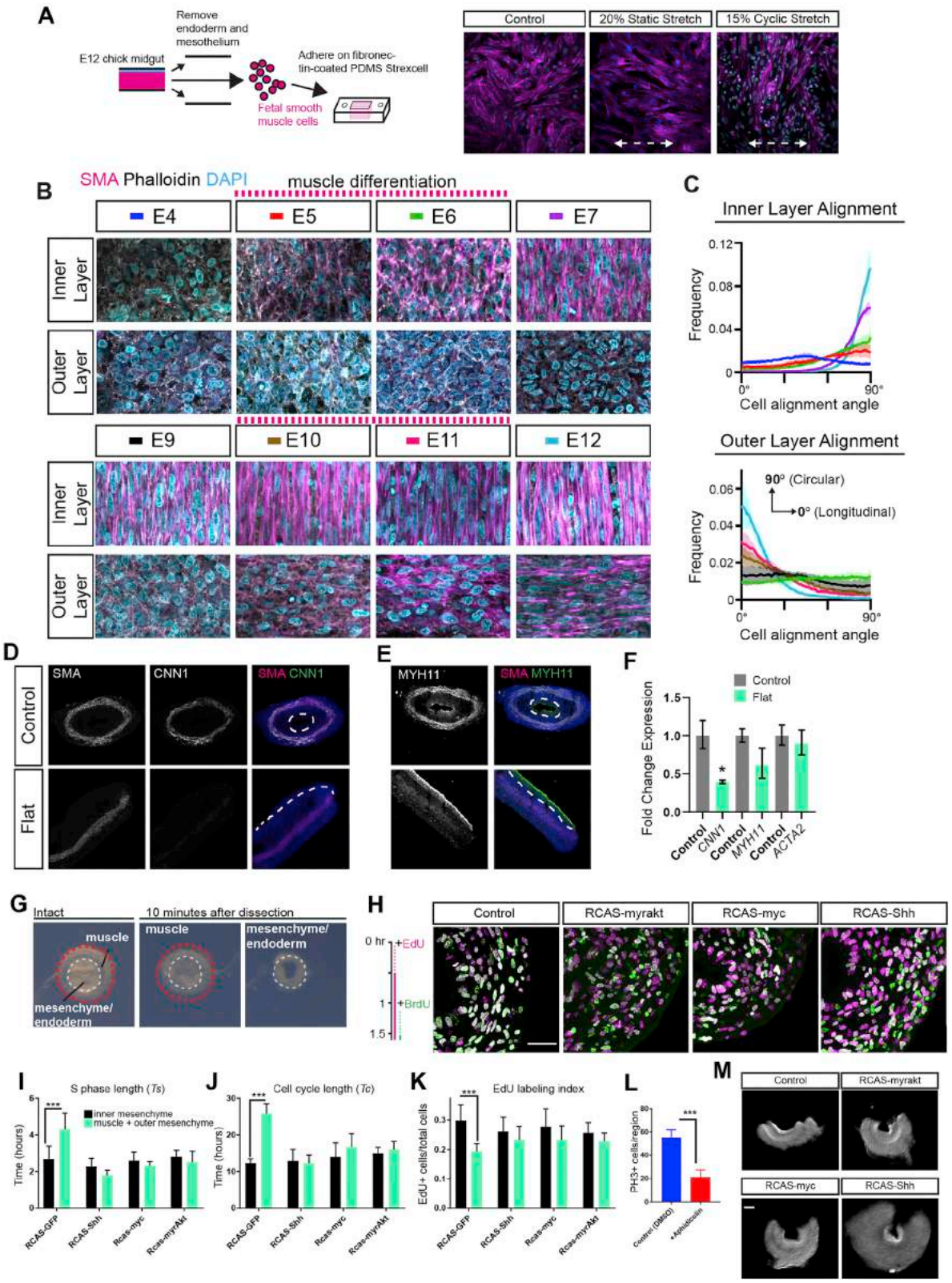

(legend on next page)

Figure S5. Strain Influences Intestinal Smooth Muscle Alignment, Related to Figures 4 and 5

(A) Scheme for isolation of chick fetal intestinal smooth muscle cells for culturing in the PDMS Strexcell chamber. When cultured without strain, smooth muscle cells do not have a preferential alignment across a population, but align locally to neighbors likely through contact guidance. Application of 20% static (continuous) stretch causes cells to align nearly parallel to the stretch axis whereas cells cyclically stretched align perpendicular. Images were taken following 96 hours in culture, arrows indicate direction of applied stretch.

(B) Time series of smooth muscle development and cellular alignment within each muscle layer of the chick small intestine (jejunum).

(C) Quantification of cellular alignment from images in (B) based on Phalloidin staining as a readout for cell orientation, as it strongly stains at cell membranes. Colors used are labeled in (B). Note that cells become aligned within each layer at the same time smooth muscle differentiation occurs and not prior to, indicating that smooth muscle maturation might be required to respond to strain. Two Z stacks each for two individual guts at each stage were used for quantification.

(D) Immunostaining for SMA and Calponin1 (CNN1) in cross sections of chick midguts cultured as tubes or cut opened (flat) for 48 hours from E5. Black and white images show separated channels.

(E) Same as (D) but stained with Myosin Heavy Chain 11 (MYH11). Note that the endoderm staining is an experimental artifact. Images are representative of 4 explants per treatment.

(F) Relative expression of noted smooth muscle markers from guts cultured as in (D), either as control tubular geometry or cut opened and flat. Fold change was determined relative to *GAPDH*. $*p < 0.05$ with unpaired t test. Error bars are mean ± SEM.

(G) Microdissection of E6.5 chick midgut. The muscle layer reduces in inner/outer circumference when dissected away from the mesenchyme and endoderm, while these layers expand in circumference, indicating that the muscle is tensed and mesenchyme/endoderm compressed.

(H) Sections from EdU/BrdU pulse labeling in chick at E6.5 demonstrating increase frequency of EdU-only cells, indicative of a faster S-phase, in guts infected with viruses misexpressing pro-proliferative factors.

(I-K) Quantitation of sections from (H), for S-phase length (I), total cell cycle length (J), and fraction of EdU-labeled cells (K) (See STAR Methods for details).

(L) Quantification of phosphor-histone H3 positive cells in a 212x212x50μm region of interest from whole mount stains in Figure 4.

(M) Whole mount 300 μm segments from the ileum of E7 midguts from control or electroporated and infected guts cut radially.

Error bars are mean ± SD, $***p < 0.001$ by two tailed t test. Scale bars = 50μm.

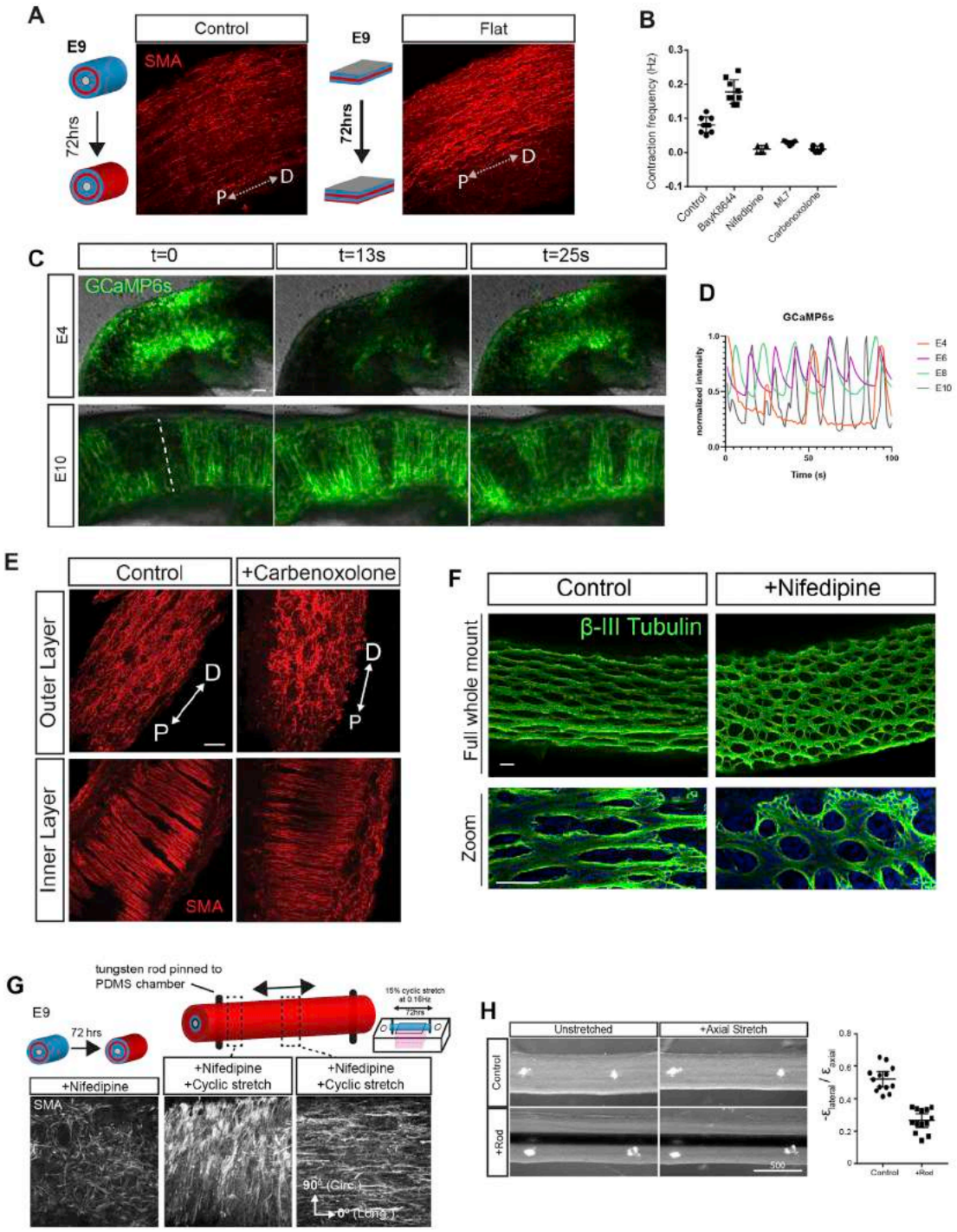

Figure S6. Alignment of the Second Layer Is Dependent upon Cyclic Contractions, Related to Figure 5

(A) Whole mount of E9 midgut stained with SMA after being grown flat for 72hrs shows longitudinal alignment similar to controls grown in standard tubular geometry. Arrows denote proximal-distal axis.

(B) Contraction frequency calculated from time-lapse analysis of explanted midgut segments. Each point represents the average of 3 measurements from 3 distinct points within the jejunum of an individual explant over a 2 minute period taken after 24 hours in culture from E9 (0 = no detectable contractions over a 2 minute observation period). Error bars are mean ± SD.

(C) Images from time-lapse analysis of calcium dynamics using RCAS-GCaMP6S over specified time (in seconds) of E4 and E10 midgut segments in explant culture. At E4 calcium transients are already present, showing whole segments of the gut that illuminate in a pulsatile fashion. By E10, these calcium transients

(legend continued on next page)

have evolved into waves that propagate in both proximal-to-distal and distal-to-proximal directions. These waves of calcium influx correspond with circumferential contractile ripples that move in both directions.

(D) Traces of GCaMP6S from time course analysis as in (C) at specified stages. Note the presence of cyclic calcium influx from an early stage (pre muscle differentiation at E4). Fluorescence intensity was measured by calculating the mean intensity every second for 100 s within an ROI generated by drawing a line across the midgut along the circumferential axis (shown as dashed line in (C) for example).

(E) Whole mount of outer and inner layers of midgut treated with carbenoxolone (100μM) from E9 for 72 hours. Note that the loss of alignment of the outer layer we observe when contractions are inhibited, as opposed to the acquisition of a circumferential alignment by default, is likely due to the maintenance of the circumferential layer, which forms a stiff boundary and presumably prevents tissues on the outside from being stretched.

(F) Whole mount images of the myenteric plexus stained with β-III Tubulin in explanted jejunal segments from chick midguts cultured from E9 for 72 hours in the presence or absence of 100μM Nifedipine. Control guts show mainly longitudinal distribution of projections between ganglia, while this pattern is perturbed in guts treated with nifedipine and ganglia additionally appear closer together and less organized.

(G) Whole mount images of midgut explants treated with nifedipine from E9 for 72 hours and stretched 15% cyclically at 0.1667Hz. Cells align perpendicular at ends of segment and parallel in center of segment to axial stretch.

(H) Whole mount images of live guts labeled with DiI and stretched ~15% longitudinally with or without a 0.005 inch tungsten rod inserted through the lumen. Graph shows measurements for ratio of lateral strain to axial (longitudinal) strain. Each point represents the average of 4 measurements across an individual stretched midgut (ileum) segment. Intubation prevents lateral compaction. Error bars are mean ± SD. Scale bars = 50μm (A-D), 500μm (E).

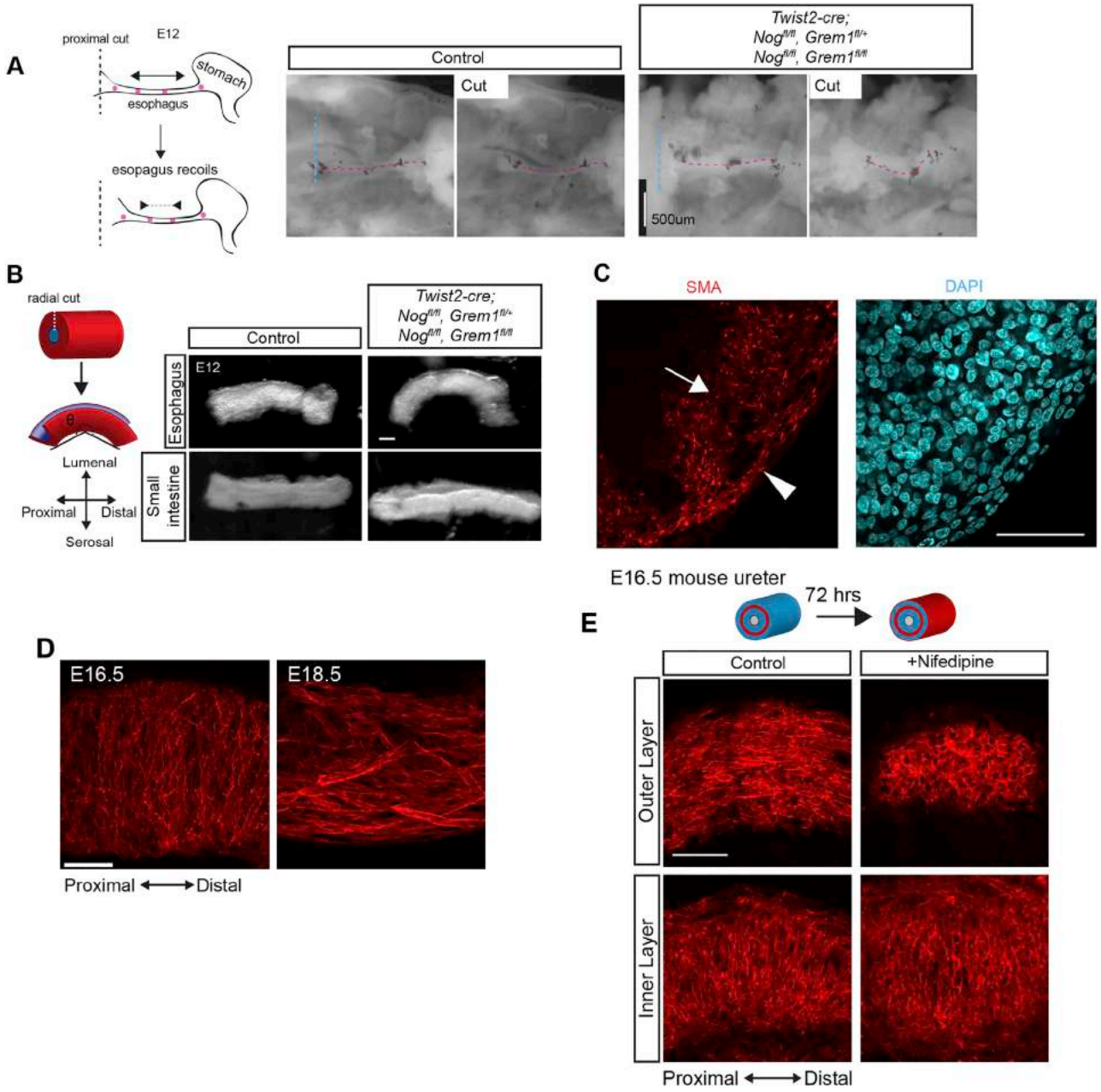

Figure S7. Mechanical Forces Align Smooth Muscle in the Mouse Esophagus and Ureter, Related to Figure 6

(A) Example of extensional strain measurements in mouse esophagi for both controls and mutants. Left images show the esophagus still attached to the mouth and stomach, but with connective and airway tissue removed. Right images show the result after a proximal cut is made at the proximal esophagus.

(B) Lateral views of E12 mouse esophageal (top) and jejunal (bottom) segments cut open radially along their length shown for both controls and Noggin/Gremlin conditional mutants. When opened, the esophagus, but not the intestine, bends longitudinally indicating that inner layers are compressed longitudinally and outer layers tensed longitudinally.

(C) Transverse cross section of inverted gut from experiment in Figure 6E showing inverted outer circumferential layer (arrowhead) and inner longitudinal layer (arrow). DAPI also shown to demonstrate spindle shaped nuclei in circumferential direction within the outer layer and rounded nuclei within the inner layer (and thus spindle shaped along the longitudinal axis).

(D) Whole mount of wild-type ureters showing inner circumferential muscle layer at E16.5 and outer longitudinal layer at E18.5. (E) Whole mount of ureter explants grown from E16.5 for 72 hours with DMSO (Control) or 50μM nifedipine. Scale bars = 50μm.